UNIVERSIDADE
BEIRA INTERIOR

Lightweight skins for UAV wings

(Versão final após defesa)

Rodrigo Barata Correia

Dissertação para obtenção do Grau de Mestre em
Engenharia Aeronáutica
(Mestrado integrado)

Orientador: Prof. Doutor Pedro Vieira Gamboa

Julho de 2023

Declaração de Integridade

Eu, Rodrigo Barata Correia, que abaixo assino, estudante com o número de inscrição 39925 do Curso de Engenharia Aeronáutica da Faculdade de Engenharias, declaro ter desenvolvido o presente trabalho e elaborado o presente texto em total consonância com o **Código de Integridades da Universidade da Beira Interior**.

Mais concretamente afirmo não ter incorrido em qualquer das variedades de Fraude Académica, e que aqui declaro conhecer, que em particular atendi à exigida referenciação de frases, extratos, imagens e outras formas de trabalho intelectual, e assumindo assim na íntegra as responsabilidades da autoria.

Universidade da Beira Interior, Covilhã 18 / 07 / 2023

Assinado por: **Rodrigo Barata Correia**
Num. de Identificação: 30024606
Data: 2023.07.18 17:56:40+02'00'

Dedicatory

To my parents, Fernanda and João, and my sister Margarida.

”Listen to the dictates of the heart consciously reducing importance as you go; allow yourself to have, and you will receive anything your heart desires”

Zeland Vadim

Acknowledgements

I would like to acknowledge everyone who gave me support and courage in the course of my academic years and throughout the work done in this thesis.

To my supervisor Professor Pedro Gamboa, the person I was sure it would be able to support me throughout my thesis, not only for the knowledge he was able to pass on to me over the years, but also for his patience and willingness to help me.

To my mom Fernanda Barata, my dad João Correia and my sister Margarida Correia, for their major support and advice, for the long trips they took across the country to see me and for always pushing me forward and encourage me to be a better version of myself everyday.

Resumo

Este trabalho investiga diferentes métodos de produção e o comportamento mecânico e elástico de estruturas de sanduíche em compósito sob esforços de flexão. Materiais de tecido de fibra como fibra de carbono e materiais de núcleo como espuma Airex, madeira de balsa e estruturas de favo de mel são analisados em diferentes configurações, tanto experimentalmente quanto computacionalmente.

O principal objetivo deste estudo é identificar qual a sanduíche em compósito que possui melhores propriedades mecânicas e pode ser usada nas cascas de asas para aviões de pequenas dimensões como UAVs. Para isso, foi realizado um ensaio de flexão em três pontos, seguido de uma simulação estrutural em ANSYS® para validar os resultados obtidos.

As amostras testadas têm uma espessura relativamente baixa para serem adequadas para pequenos UAVs (menos de 2.5 mm). Todas as amostras foram produzidas com duas camadas de tecido de fibra de carbono com $30\ g/m^2$ em cada lado da sanduíche e um material de núcleo. A sanduíche de madeira de balsa foi a amostra mais eficiente com uma resistência por unidade de massa de $11.49\ N/g$ e também a mais rígida com um módulo de flexão de $3.18\ GPa$. A sanduíche de espuma AIREX® C 70.75 foi a amostra com menor eficiência com uma resistência por unidade de massa de $5.91\ N/g$ e também a menos rígida com um módulo de flexão de $0.86\ GPa$. A sanduíche de Nomex® honeycomb orientado na direção longitudinal e transversal tinham uma resistência por unidade de massa de $9.62\ N/g$ e $9.11\ N/g$ e um módulo de flexão de $1.00\ GPa$ e $1.08\ GPa$ respectivamente.

Embora os resultados da análise de elementos finitos não tenham sido satisfatórios, os procedimentos experimentais e as experiências foram realizadas com sucesso e dados suficientes foram coletados para tirar conclusões confiáveis sobre o uso da estruturas de sanduíche em compósito mais adequada para asas de UAV, sendo a sanduíche de madeira de balsa a com o melhor desempenho no geral.

Palavras-chave

Sanduíche em compósito, flexão em três pontos, fibra de carbono, UAV, rigidez à flexão, cascas leves, FEA.

Abstract

This work investigates different production methods and the mechanical and elastic behavior of composite sandwich structures under bending stress. Fiber cloth materials like carbon fiber and core materials like Airex foam, balsa wood, and honeycomb structures are analyzed in different layups both experimentally and computationally.

The main objective of this study is to identify which composite sandwich has better mechanical properties and can be used as a lightweight structure for the wing skin of small airplanes like UAVs. For that, a three-point bending test was performed and followed by a structural analysis simulation in ANSYS® to validate the results obtained.

The samples tested have a relatively low thickness in order to be suitable for small UAVs (less than 2.5 mm). All of the samples were produced with two layers of a lightweight $30\ g/m^2$ carbon fiber cloth on each side of the sandwich and a core material. The balsa wood sandwich was the most weight-efficient sample with a strength per unit of mass of $11.49\ N/g$ and also the most rigid with a flexural modulus of $3.18\ GPa$. The AIREX® C 70.75 foam sandwich was the least weight efficient sample with a strength per unit of mass of $5.91\ N/g$ and also the least rigid with a flexural modulus of $0.86\ GPa$. The Nomex® honeycomb core sandwich oriented in the lengthwise and widthwise direction had a strength per unit of mass of $9.62\ N/g$ and $9.11\ N/g$ and a flexural modulus of $1.00\ GPa$ and $1.08\ GPa$ respectively.

Even though the finite element analysis results were not satisfactory, the experimental procedures and experiments were successfully performed and enough data was collected in order to take reliable conclusions concerning the use of the most adequate lightweight sandwich structure for UAV wings with the balsa wood sandwich being the one with the better overall performance.

Keywords

Composite sandwich, three-point bending, carbon fiber, UAV, bending stiffness, lightweight skins, FEA.

Table of Contents

List of Figures

List of Tables

Acronyms

ASTM	American Society of Testing Materials
CAD	Computer-aided design
CFRP	Carbon fiber reinforced polymers
DGEBA	Diglycidylether of bisphenol A
FE	Finite element
FEA	Finite element analysis
ISO	International Organization for Standardization
PEEK	Poly-ether-ether-ketone
PP	polypropylene
PPS	polyphenylene sulfide
PVC	Polyvinyl chloride
RAM	Random access memory
UAV	Unmanned aerial vehicle
UBI	University of Beira Interior
WHO	World Health Organization

Nomenclature

$\Delta\sigma$	Stress variation
$\Delta\varepsilon$	Strain rate variation
ΔP	Load variation
Δs	Vertical displacement variation
γ_f	Fiber surface mass
ν_{12}	Poisson ration in the primary direction
ν_{23}	Poisson ration in the secondary direction
$\bar{x}$	Sample mean
ρ	Density
ρ_f	Fiber density
σ	Stress
σ_1	Stress at point 1
σ_2	Stress at point 2
σ_f	Flexural stress
τ	Shear stress
τ_c	Core shear stress
τ_f	Facing shear stress
ε	Strain rate
ε'	Strain rate at the initial point
ε''	Strain rate at the final point
ε_1	Strain rate at point 1
ε_2	Strain rate at point 2
b	Sandwich width
c	Core thickness
$C_{V,R}$	Relative cost per unit volume
CV	Coefficient of variation
d	Sandwich thickness
E	Modulus of elasticity
E_1	Modulus of elasticity in the primary direction
E_2	Modulus of elasticity in the secondary direction
E_B	Bending modulus of elasticity
G	Shear modulus
h	Laminate thickness
l	Sandwich length
L	Support length
m	Slope
m_s	Specimen mass
n	Number of tested specimens
n_{plies}	Number of plies in a cured laminate
P	Load

P'	Load at the initial point
P''	Load at the final point
P_{max}	Maximum load
r	Lower support radius
R	Upper support radius
S	Shear strength
s	Vertical displacement
s'	Vertical displacement at the initial point
s''	Vertical displacement at the final point
S_{n-1}	Sample standard deviation
t	Thickness
t_{ply}	Thickness of a single cured ply
t_c	Core thickness
t_f	Facing thickness
V_f	Fiber volume fraction
x	Measured value of a single observation
X_c	Compressive strength in the primary direction
X_t	Tensile strength in the primary direction
Y_c	Compressive strength in the secondary direction
Y_t	Tensile strength in the secondary direction
z	Cross-head loading rate

Chapter 1

Introduction

This chapter has the main purpose of contextualizing the work done through this thesis with its relevance along different times of the aeronautical engineering past, present, and future. It also serves to present the main inspiration and objectives behind this research and its layout.

1.1 Historical background

1.1.1 Composite Structures

The urge to produce better quality materials can be seen on many occasions during the evolution of humanity. Back in 3400 BC, the Mesopotamians were the ones to first use composite sandwiches. These ancient people glued wood strips at different angles to create plywood. Similar techniques to create stronger structures can also be seen in 1500 BC when the Egyptian artisans and builders used straw to reinforce boats, mud bricks and pottery [1]. In today's society, we call this a composite structure.

Metals, ceramics, and polymers are the three main kinds of material that can make up a composite. In addition to incorporating the greatest qualities of each of the component elements, the design objective of a composite is to attain a combination of properties that no single material can demonstrate. Diverse assemblages of metals, ceramics, and polymers serve as representations for a wide variety of composite kinds. Additionally, some naturally occurring materials, like wood and bone, are composites. However, the majority of those that are taken into account are artificial (or man-made) composites. As shown in Figure 1.1 different classifications can be attributed to a composite structure depending on its reinforcement nature.

To promote the safety of a population, the defense sector is always evolving and only in this way it is possible to outbalance any external harm attempts. At these times, it is expected for a nation to spend large amounts of resources as a means to defend its own interests. These resources may include everything from materials, food, and military personnel. As a result, technological development is typically accelerated to solve specific military needs which later can evolve into non-military equipment. A good example of that is the evolution of composite materials.

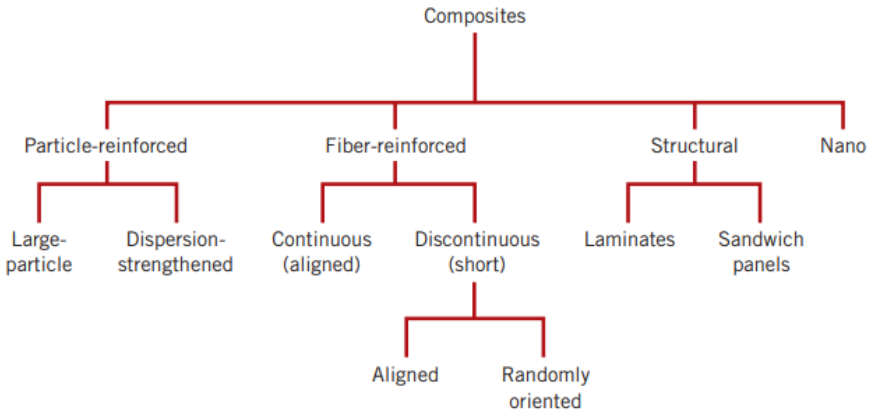

Figure 1.1: Classification scheme for composite structures according to their reinforcement [2].

In the 1930s a researcher in a U.S. company called *Owens-Corning*, accidentally blew a jet of compressed air into a stream of molten glass producing something similar to fiber strips. After this discovery, extensive research was conducted in order to commercialize fiber-reinforced plastics.

In 1939 the demand for defense equipment was dramatically increasing and having better air equipment was more important than ever. Therefore, the focus on making stronger, safer, more fuel-efficient (and therefore lighter) aircraft was a global priority. It was a year later when in 1940 *de Havilland Mosquito* (Figure 1.2), the first airplane with composite structures, was developed by the British aviation manufacturer *de Havilland*. This fighter-bomber had a plywood-balsa-plywood monocoque-sandwich shell construction which gave an excellent aerodynamic performance, low weight, and increased strength and stiffness [4]. Quickly after, *Owens-Corning* began producing fiberglass and polyester airplane parts which were plastic laminates made from fiberglass fabric impregnated with resin.

Figure 1.2: First airplane with composite structures - de Havilland Mosquito [4].

Lightweight skins for UAV wings

Although fiber-reinforced materials started being used in 1939, they were not extensively manufactured until the 1960s with the discovery of the strength potential of carbon fiber matrices by Dr. Shindo's research [5]. Not many years later, on 20 July 1969 and for the first time, with the big outstanding progress made in science, a spaceship successfully landed on the moon. Even though public interest centered on rocketry and computer technology, it was only with the help of sandwich technology that a shell of the spacecraft was able to be lightweight and still strong enough to sustain the stresses of acceleration and landing. Figure 1.3 shows on the left side the wall construction of the Apollo capsule which consisted of two interconnected sandwich shells. Details of the outer shell, which comprised two thin steel facings and a honeycomb core, can also be seen on the right side of the same figure. The inherent advantage of sandwich construction is immediately apparent, namely, high strength and rigidity at low weight [6].

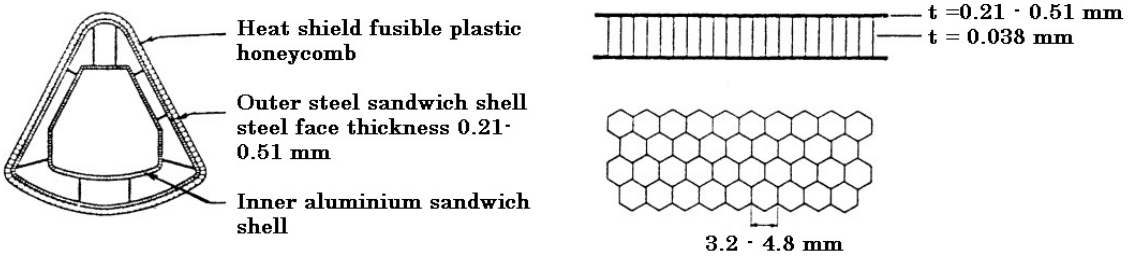

Figure 1.3: Sandwich construction of the Apollo capsule (left) and cellular sandwich forming the outer shell of the Apollo capsule (right) (adapted from [6]).

It is crucial to understand that since each type of material was first used in airplanes, advances have been made continuously. For instance, since the 1920s, advances in aluminum alloys have been made to enhance qualities like strength, hardness, and corrosion resistance. Similar improvements in composite materials have increased mechanical characteristics and impact toughness while decreasing costs since the 1970s [7]. The progress made in composite structures led aircraft manufacturers to race for the implementation and replacement of more conventional and well known materials like aluminum and steel by new and more efficient materials in the composites family. Figure 1.4 shows how the usage by mass of composite materials has increased and the use of metal has decreased through time on significant Boeing commercial aircraft.

1.1.2 Unmanned aerial vehicles (UAVs)

With the advancements made in technology and autonomous vehicles, unmanned aerial vehicles have been used in a wide range of applications such as security, surveillance, emergency response, mapping, monitoring of wild life and catastrophes, deliveries, agriculture, videography and so on.

All systems used in aerospace must be lightweight and cannot operate at peak performance without the right materials. The more efficiently a structure performs, the lighter the aircraft gets, the heavier the payload it can carry, the greater the range it can travel and the

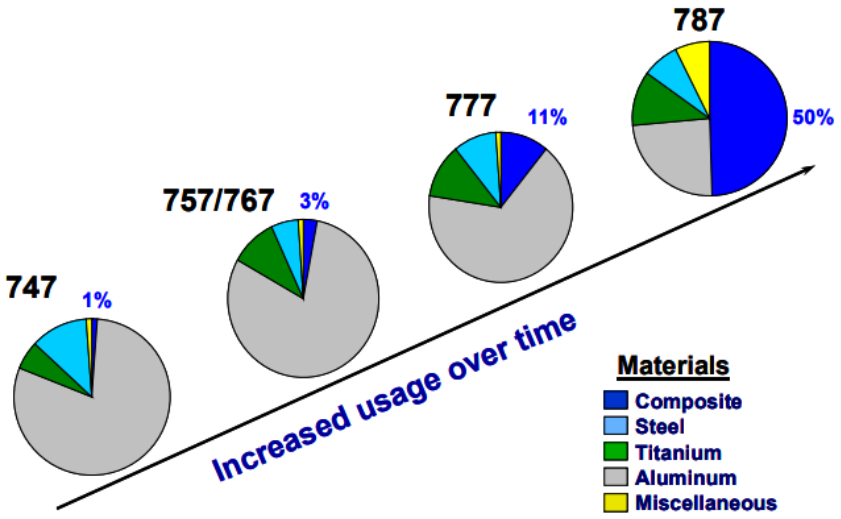

Figure 1.4: Increase in usage of composites in Boeing commercial aircraft over time [8].

longer it can stay in the air. UAVs must have sensors, cameras, and electronics in order to fly unmanned but in a minimum weight perspective, the biggest concern is normally the propulsion system. Small UAV drones are mostly powered by batteries, which represent a large percentage of the total weight of the aircraft and consequently, there is an increased need to lighten any other systems. That is why lightweight composite skins, made with advanced materials like carbon fiber and composite sandwiches, have become so popular among manufacturers of UAVs. The development of these composite structures has led to more weight-efficient wings that reflect a less need of energy usage during flight and therefore, makes them better suited for the task.

The Bayraktar TB2 (Figure 1.5) is a medium-altitude long-endurance UAV manufactured by the Turkish company *Bayar*, for the Turkish Armed Forces. Fuselage pieces and wing structures are mostly made of carbon fiber composites.

Figure 1.5: Baykar Bayraktar TB2 Turkish UAV [9].

1.2 Scope and motivation

From prehistory, passing through the middle ages, and coming to our modern eras, the improvement made by scientists and researchers in the pursuit of achieving superior, better quality, more efficient, and stronger materials have been a constant. As a result, the demand for composite structures in the aviation sector has increased significantly in the last few years. From a cost-effective perspective, advanced composite structures are very reliable, they lead to less weight, increased fuel efficiency, lower prices, and guarantee good structural stability. All of these factors led to an increased interest from academia and industry to explore the capabilities of composites even further.

With the discovery of the SARS-CoV-2 virus in late 2019 and with its mighty spreading rate across the globe, the World Health Organization (WHO) declared on 11 March 2020 the start of the COVID-19 pandemic. This outbreak came with a severe negative impact on the aviation industry market due to a lack of raw materials, supply chain disruptions, travel restrictions, operational challenges, and transportation delays. On market research conducted by *Polaris Market Research* (Figure 1.6), it is possible to see an abrupt drop in the market value for composite structures due to the COVID-19 pandemic. Nevertheless, it is expected that the industry keeps growing over the next few years as technologies keep getting more advanced and more improvements are made in order to achieve better-quality composite materials.

This work was motivated by the necessity to obtain and reliably produce lighter and stronger materials for UAV wing skins, in particular, sandwich composite structures made out of carbon fiber-reinforced polymers (CFRP) and very lightweight cores.

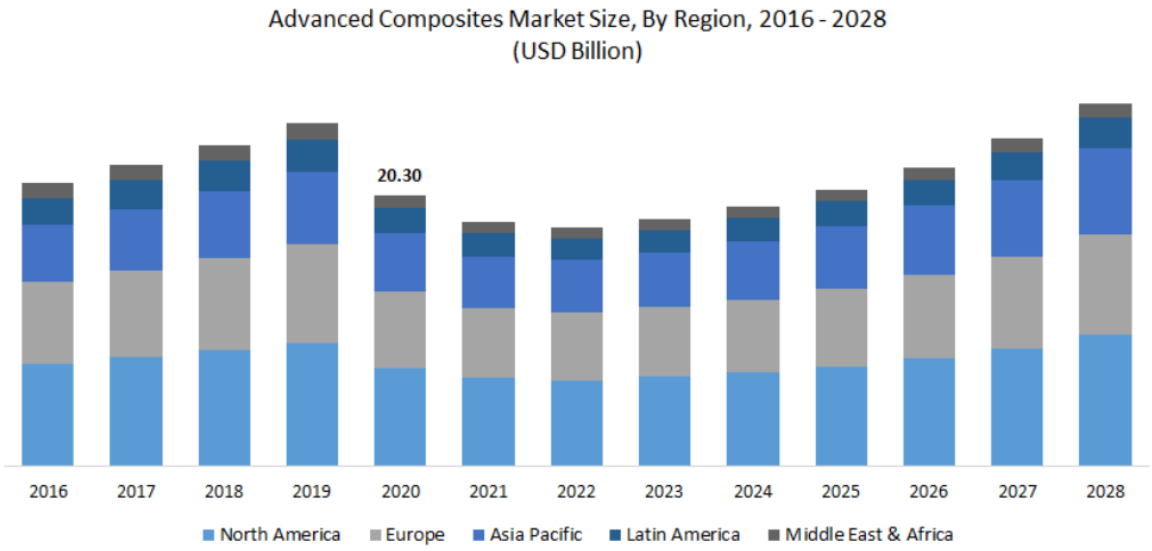

Figure 1.6: Advanced composites market forecast by region, 2016 - 2028 by Polaris Market Research [10].

1.3 Objectives

The main focus of the work developed in this thesis is to get a better understanding of the different materials used in thin walled parts of small aircraft or UAVs and to enable the replication of the methods described in order to get the most suitable composite sandwich structure for the application. In order to achieve this goal, a set of objectives were proposed:

1. Identify state of the art core materials suitable for composite sandwich laminates
2. Predict the elastic behavior and failure of different composite sandwiches
3. Experimentally evaluate the mechanical properties of composite sandwich samples
4. Validate the experimental results with finite element analysis (FEA)

1.4 Research methodology

The aim of this section is to give a layout in which this work will be guided from.

The work developed in this thesis is divided into six main chapters which will set apart different topics into relevant information for this work.

Chapter 1 - **Introduction**, has the main purpose of contextualizing the work done through this thesis with its relevance along different times of the aeronautical engineering past, present, and future. It also serves to present the main inspiration and objectives behind this research and its layout.

Chapter 2 - **State of the Art**, aims to give a detailed review of the literature in the field of composite sandwich structures and it represents the latest or most advanced techniques, methods, equipment, and knowledge that are currently available in the industry and in academia.

Chapter 3 - **Experimental procedure**, describes the procedures used to conduct the experimental work and the guidelines followed to ensure valid results.

Chapter 4 - **Finite element analysis**, aims to give a brief explanation of what a Finite element analysis is and the main features needed to take into account when performing one. The steps and techniques used to run the simulation are also described throughout this chapter.

Chapter 5 - **Results**, presents and compares all the results obtained through the experiments done along this work.

Chapter 6 - **Conclusion**, has the main purpose of giving an overview of the conclusions taken from the work done and giving guidelines for future work.

Chapter 2

State of the Art

This chapter aims to give a detailed review of the literature in the field of composite sandwich structures and it represents the latest or most advanced techniques, methods, equipment, and knowledge that are currently available in the industry and in academia.

The state of the art is divided into four main chapters.

Section 2.1 - **Composite sandwich definition**, summarizes the main aspects of a sandwich composite structure, its components, advantages and disadvantages, and other important features.

Section 2.2 - **Materials**, describes the main difference between each material used in a composite sandwich structure, as well as the numerous possibilities for material combinations.

Section 2.3 - **Manufacturing processes**, describes in detail each manufacturing process and also their advantages and disadvantages.

Section 2.4 - **Failure modes of composite sandwiches**, describes the different failure modes that can be observed in a composite sandwich structure.

2.1 Composite sandwich definition

The phrase "the whole is greater than the sum of its parts" is very applicable to composite materials where two materials are combined to provide an overall better performance (such as strength or lighter weight) for a certain application, which would never be possible when isolating the materials.

A composite sandwich can be defined as a multilayered structure composed of two relatively thin, with high strength and stiffness laminate face sheets bonded to a lightweight core normally, foam, balsa wood, or multicellular honeycombs (Figure 2.1). All these core materials are characterized by a high stiffness-to-weight ratio, which makes them versatile and reliable for many applications in the aerospace and aeronautical engineering field.

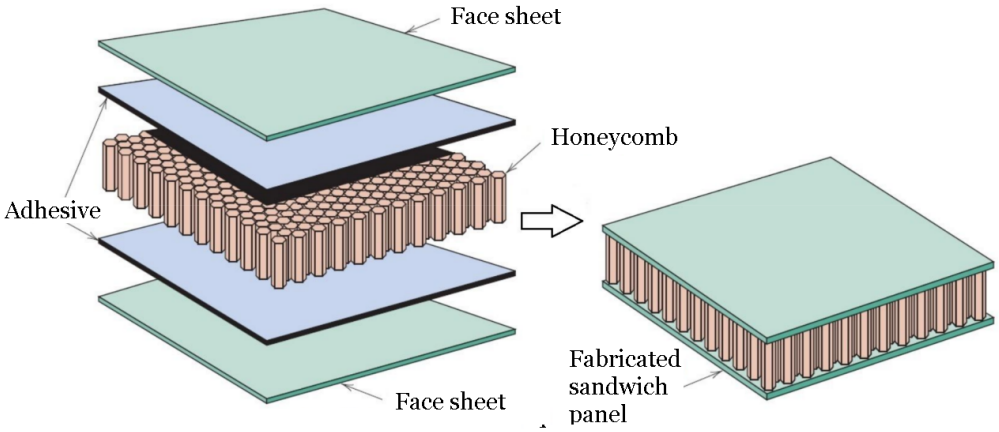

Figure 2.1: Representation of a basic sandwich structure (adapted from [11]).

The resistance of a member against bending deformation is called bending stiffness and is one of the characteristics that a composite structure greatly benefits from and is much greater than that of a single laminate face sheet with the same total weight and made of the same material as the faces of the sandwich. Although obtaining a lightweight sandwich structure may seem as easy as placing a weightless core between two extremely stiff facings, engineers can not normally do that because the facing and core materials are mutually dependent on one another to perform their function. For example, the core must be stiff enough to keep the faces nearly flat; otherwise, it is possible to occur local buckling (wrinkle) in the laminate faces under the influence of compressive stress.

Some of the benefits of composite materials include:

- Excellent thermal insulation;
- Good surface finish;
- Lighter weight and higher strength when compared to aluminum or steel;
- Possibility to achieve combinations of properties not attainable with metals, ceramic, or polymers alone.

Composite materials also have some disadvantages including:

- Generally expensive materials;
- Most of the fabrics used in laminates have different properties depending on the direction in which they are measured. This may be an advantage or disadvantage depending on the knowledge of the manufacturer;
- Polymer-based composites are subject to deprecating reactions with chemicals or solvents;
- Labor-intensive manufacturing processes.

2.2 Materials

In the early days, airplane parts were mainly manufactured from metal alloys such as aluminum and steel because of their high strength-to-weight ratio, easy manufacturability, and relatively low cost, but with today's progress made in technology and research, composite materials have become a more reliable option for even the most strength demanding structures in an airplane. One of the most important stages of any aircraft design or structure has always been its material selection. The most common criteria that engineers take into account are yield and ultimate strength, density, stiffness, thermal and electric conductivity, and corrosion resistance and although the cost is not a property, it is also considered when selecting the best material.

Figure 2.2 represents a plot of strength vs density for various materials. Composite materials like CFRP have a lower density for the same strength as many metals. Besides that, when automatized processes are not available, CFRP manufacturing can be very labor-intensive and complex. For that reason, metals like aluminum are much more preferred for their relatively easy processing and lower price, which is represented in Figure 2.3.

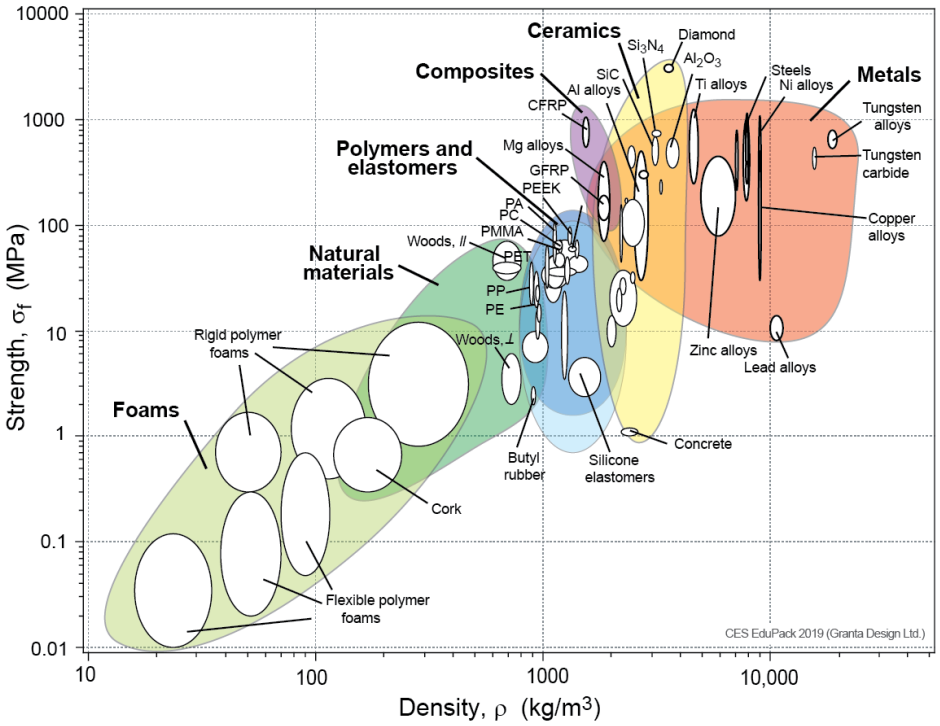

Figure 2.2: Strength vs density materials chart [12].

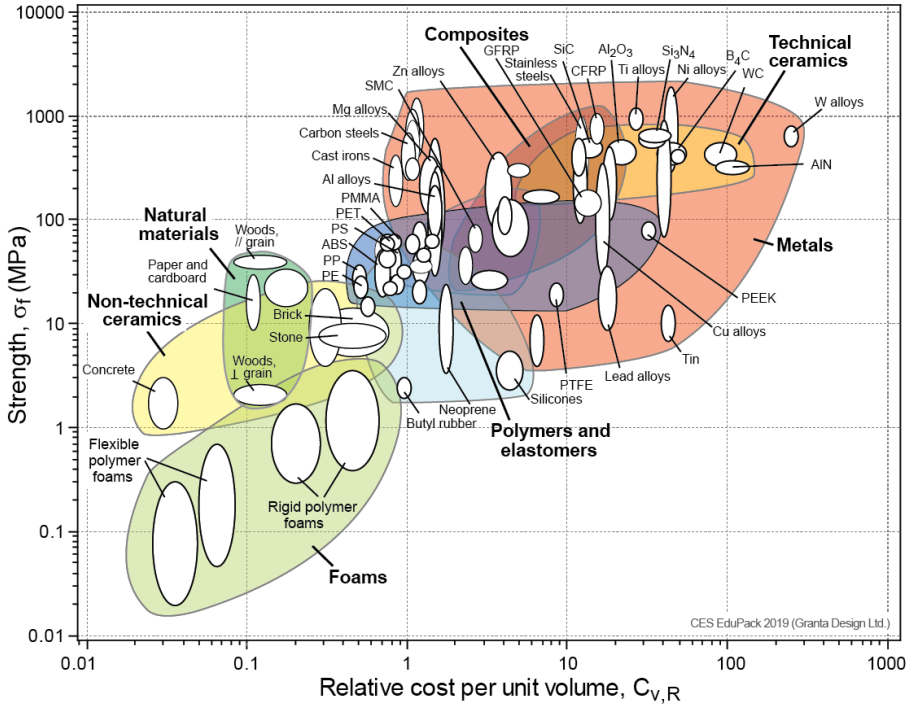

Figure 2.3: Strength vs relative cost per unit volume materials chart [12].

2.2.1 Fiber reinforcements

Fiber reinforcements are the main responsible in giving a sandwich structure its stiffness and strength, but a good knowledge and understanding of how their properties work is a key factor to getting the best out of these materials. When used as a woven fabric, this can come with either unidirectional or bidirectional fibers. Unidirectional cloth is composed of multiple fibers aligned in only one [0º] direction and has very good tensile properties along the direction of the fibers but is very weak in its perpendicular direction. On the other hand, the bidirectional cloth is composed of fibers in two perpendicular directions [0º,90º], which gives the cloth good properties in both parallel or perpendicular directions. Furthermore, bidirectional cloth can have a different pattern of interlaced regions of the orthogonal fibers, usually referred to as weave styles. The most common ones are the plain weave, twill weave, and satin weave (Figure 2.4). The drapeability of the cloth increases from plain to twill and satin weaves but as a consequence the care with each one is handled must also increase to not disorientate the fibers.

There are four main factors that govern a laminate's overall performance:

1. The mechanical properties of the fiber reinforcement itself;
2. The orientation of the fibers in the composite;
3. The surface interaction of fiber and resin (fiber and matrix adhesion);
4. The fiber to resin weight ratio.

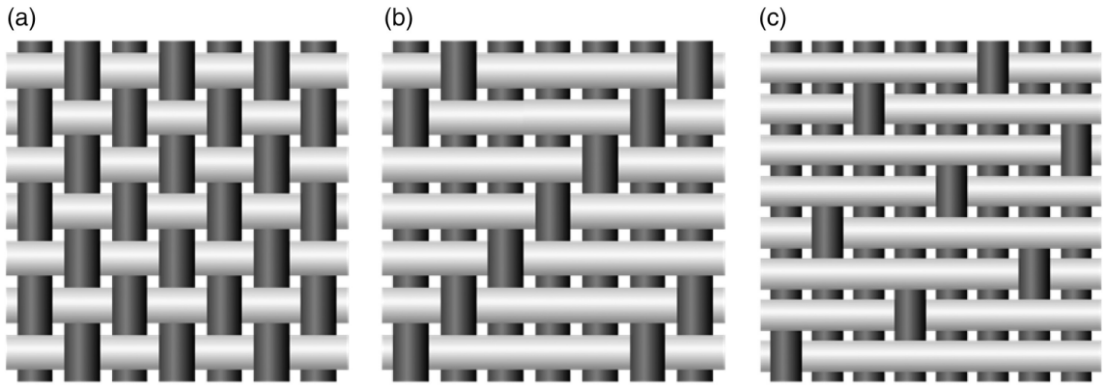

Figure 2.4: Different weave patterns of composite fabric: (a) plain weave, (b) twill weave, and (c) satin weave. [13].

Composite laminates usually have more than one layer of fibers with different orientations or materials. This usually gives the composite an overall better performance and allows for some redundancy in the structure. For example, a composite with different layers of carbon fibers and aramid fibers can benefit from both the high strength of the carbon and the great impact resistance of the aramid.

As stated before, different ply orientations are normally used in a stacking sequence. This happens as a consequence of the orthotropic nature of any composite laminate which requires the laminate to have layers orientated in [0°],[+45°,-45°], and [90°]. The [0°] and [90°] orientations usually withstand most of the tension and compression stress whilst the [+45°,-45°] orientations are responsible to withstand most of the shear stresses. This last one is normally used in wing skins where shear stresses are more predominant. Figure 2.5 represents a [0°/+45°/-45°/90°]s stacking sequence, where the letter ”s” stands for ”symmetric”.

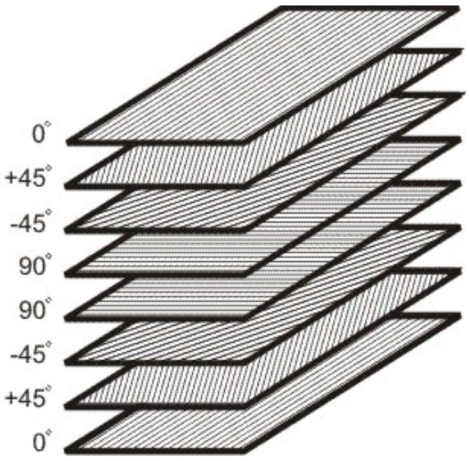

Figure 2.5: Example of a stacking sequence with plies oriented in different angles. [14].

Depending on the desired outcome, there are three main types of fiber reinforcements largely used in the aviation industry, glass fiber, carbon fiber, and aramid fiber.

Glass fiber

Glass fiber (or fiberglass) is often used on secondary structures[1] of aircraft, such as fairings, radomes, and wing tips due to its low cost, good galvanic corrosion resistance and electrical properties. Particular types of fiberglass used in the aviation industry are the E-glass, S-glass, and S2-glass, being the first one mainly used in electrical applications as a consequence of its high resistance to current flow, and the last two as structural fiberglass that has a higher strength than E-glass. Fiberglass has a white color and is available as a dry fiber fabric or prepreg material form [15].

Carbon fiber

Carbon fibers can be 3–10 times stiffer than glass fibers and they offer more reliable performance for structural aircraft applications, such as stabilizers, primary fuselage, and wing structures. Advantages include its high strength and lightweight. Disadvantages include lower conductivity than aluminum (therefore, a lightning protection mesh or coating is necessary for aircraft parts that are prone to lightning strikes), high potential for causing galvanic corrosion when used with metallic structures, and high cost. Carbon fiber's color is usually black and it is available as dry fabric and prepreg material [15].

Aramid fiber

Aramid fibers are lightweight and strong. Two types of aramid fiber are used in the aviation industry: kevlar 49 which has a high stiffness and kevlar 29 which has a low stiffness. An advantage of aramid fibers is their high resistance to impact damage, so they are often used in areas prone to impact, such as the wing's leading edge. The main disadvantage of aramid fibers is their general weakness in compression. Another disadvantage is that Kevlar is difficult to drill and cut. The fibers fuzz easily, and special scissors are needed to cut the material. Kevlar is often used for military ballistic and body armor applications. It has a natural yellow color and is available as dry fabric and prepreg material [15].

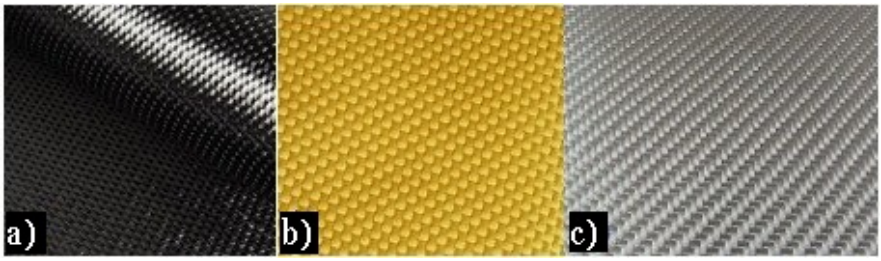

Figure 2.6: Different types of fabric extensively used in the aeronautical industry. a) Carbon fiber, b) Aramid fiber, c) Glass fiber [16].

[1]Structures whose failure can compromise the operation of the aircraft but not its structural integrity, as opposed to a primary structure.

2.2.2 Sandwich Cores

The term “Sandwich core” is normally used because these materials are sandwiched between fiber reinforced layers. They are utilized to build strength and stiffness by adding thickness to the sandwich and therefore, increasing the sectional area of the structure without adding significant weight. Most of the core materials fall into the category of either wood cores, foam cores, or honeycomb cores, which, over the years, have exhibited an increasing interest in the aviation industry. Figure 2.7 shows a close representation of these three configurations.

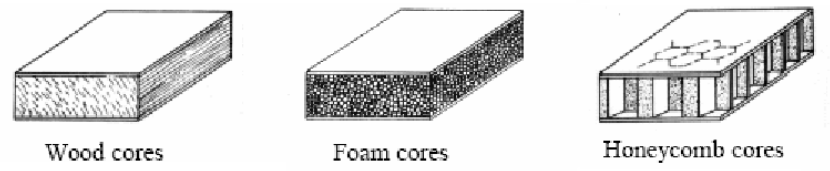

Figure 2.7: Composite sandwich structures with different core materials [17].

Wood cores

Wood is a natural core that can be easily found and worked with. The two most commonly used wood materials are plywood and balsa. Plywood is used instead of other wood materials as a consequence of its high strength, and resistance to cracking, shrinkage, and twisting. However, all wood cores are sensitive to moisture, and will eventually rot if not surrounded by epoxy resin.

Balsa wood is a very popular wood core that has been always used in the aviation industry. It exhibits very low density (for wood) and some water resistance. It also provides good thermal insulation and good acoustic absorption. It is easily formed with simple equipment and its density normally ranges from 100 kg/m^3 to 200 kg/m^3. Even though its density can be as low as one-fourth of a regular wood, it is still considered a high-density sandwich core when compared to honeycomb structures and other lightweight foams.

Foam cores

Foam cores are one of the most inexpensive and easy-to-work-with core materials. Their mechanical properties are typically isotropic and a variety of foam materials can be used as cores including [18]:

- Polystyrene (Also known as styrofoam);
- Phenolic;
- Polyurethane;
- Polypropylene;
- Polyvinyl chloride (PVC), under the tradenames Divinycell, Klegecell, and Airex;
- Polymethacrylimide, under the tradename Rohacell.

Polystyrene foam is the least expensive but has relatively low mechanical properties. Phenolic foam on the other hand, has very good fire-resistant properties and can have very low densities, but it has relatively low mechanical properties as well. Polyurethane foam is relatively inexpensive and is used primarily in automotive applications, requiring moderate structural properties. Polypropylene foam is used primarily in automotive applications requiring more demanding structural properties. Polyvinyl chloride (PVC) foam is used primarily in the marine industry but is also used as a low-price foam in the aviation industry. Polymethacrylimide foam is much more expensive than the other types of foams but has greater mechanical properties and is used primarily in the aerospace and aviation industries [18].

Honeycomb cores

A honeycomb core refers to a structure similar to what can be seen in a beehive and it can be described as an array of identical prismatic cells, normally hexagonal, which are joined together to form a plane structure. Among sandwich cores, the honeycomb structure offers the best strength-to-weight ratio and it can be manufactured from, kraft paper, thermoplastics, aluminum, steel, aramid fiber, glass fiber, carbon fiber, and ceramic. Although the aluminum honeycomb offers the best mechanical properties, it can easily be prone to galvanic corrosion when placed in contact with carbon fiber, and a good solution to this problem is to replace it with an aramid fiber honeycomb.

Most honeycomb cores are anisotropic, in other words, their properties are different depending on which direction they are measured from. Figure 2.8 represents the main orientation and directions L, W, and T of a honeycomb. The highest compressive and tensile strength of a honeycomb is in the T direction so the faces of a sandwich structure are usually placed in its normal direction, other directions are substantially weaker.

The most important strength properties used to quantify honeycomb are [18]:

- Compressive strength, either as bare core or stabilized with facings;
- Compressive modulus measured as stabilized with facings;
- Crush strength for energy absorption applications;
- Shear strength and modulus in the L and W directions.

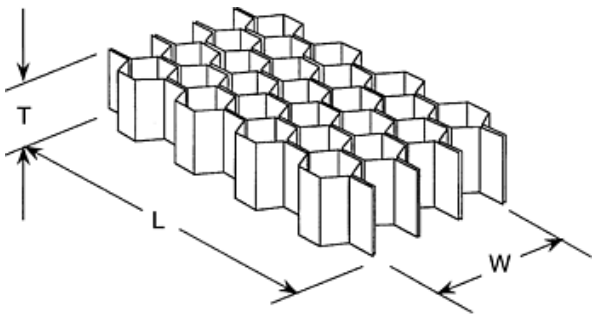

Figure 2.8: Honeycomb orientation: L (length), W (width), and T (thickness) directions [18].

2.2.3 Matrices

Contrary to fiber reinforcements, matrices have a minor role in carrying loads in a composite laminate, nonetheless, they are of great importance for the integrity of the structure. Some of the main roles of the matrix in a composite are [19]:

1. To keep the fibers in the desired position and orientation;
2. To transfer stresses to the fibers;
3. To protect the fibers from chemicals and moisture;
4. To protect the fiber's surface from mechanical degradation (e.g., by abrasion).

The three main types of matrix materials are polymer matrices, metallic matrices, and ceramic matrices. Among the polymer matrices, thermoset polymers such as epoxies represent a large percentage of the matrix materials used for long fiber-reinforced composites. Compared to polymer matrices, metal matrices have higher yield strength and modulus which can be of great importance in applications requiring high transverse and compressive strength, however, they tend to have high densities and are prone to corrosion at the fiber-matrix interface. Ceramic matrices have good thermal properties, high hardness, high corrosion resistance, and low density but they also come with their disadvantages. Some of the most critical are that these matrix materials are very brittle and have a low resistance to crack propagation [19].

Repeated units of the same or different atoms joined together by covalent bonds in long-chain molecule form what we call a polymer. These polymers can be divided into two categories: thermosets and thermoplastics. When selecting which one is the most adequate for a high-performance composite, the primary consideration should be its mechanical properties. The most desirable include [19]:

1. High tensile modulus, which influences the compressive strength of the composite;
2. High tensile strength, which controls the intraply cracking in a composite laminate;
3. High fracture toughness, which controls ply delamination and crack growth.

Thermosets, also known as thermosetting resins, include epoxies, polyesters, vinylesters, bismaleimides, and polyamides. Because of their three-dimensional cross-linked structure, thermosets tend to have high dimensional stability, high-temperature resistance, and good resistance to solvents and although they do not melt upon reheating, they start decomposing at high temperatures [20]. Epoxies make up the greatest percentage of thermoset resins used in advanced composites. They have low shrinkage during cure, promote excellent adhesion to a great variety of fibers, and possess excellent resistance to chemicals and solvents [19]. The most highly developed of the thermoset polymers are epoxies of DGEBA type (diglycidyl ether of bisphenol A). They have better mechanical and thermal properties than polyesters and depending on the type of hardening agent they can come in different stiffnesses as shown in Figure 2.9 where the higher modulus tends to be used in a high-performance component such as aircraft structures [21].

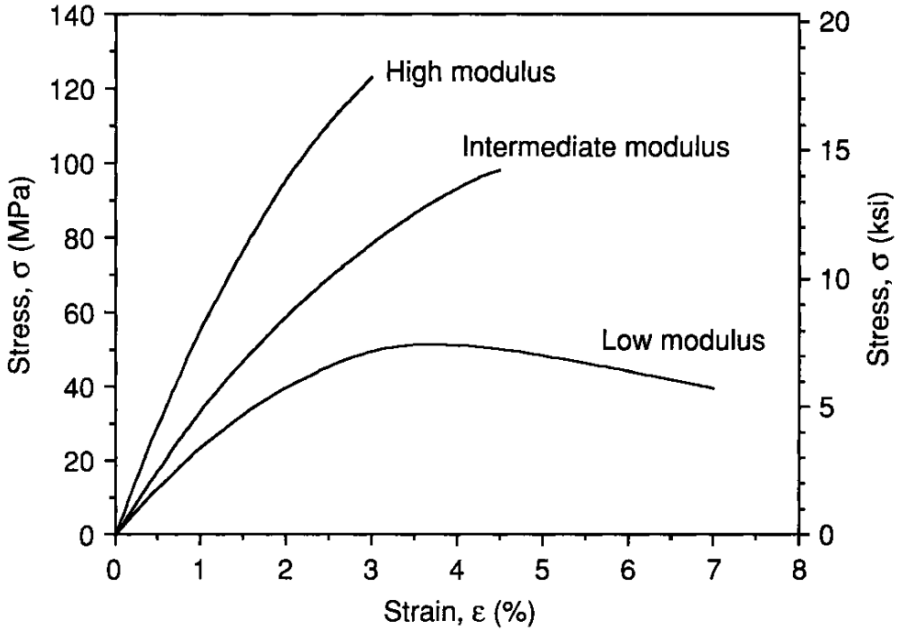

Figure 2.9: Stress vs strain curves of epoxy resins of different moduli [21].

A thermoplastic polymer does not have its molecules chemically joined together. They are held in place by weak secondary bonds or inter-molecular forces, such as hydrogen bonds and van der Waals bonds. With the application of heat, these secondary bonds in a solid thermoplastic polymer can be temporarily broken and the molecules can now be moved relative to each other or flow to a new configuration if pressure is applied on them [19]. Thermoplastics used as matrices for composites include polyphenylene sulfide (PPS), polypropylene (PP), poly-ether-ether-ketone (PEEK), polysulfone, and thermoplastic polyimides which are more compatible with hot-forming and injection molding fabrication methods [21].

2.3 Manufacturing processes

Besides all the benefits composite structures may have, their main drawback is labor intense and complex manufacturing processes. Some of the most known are hand lay-up, vacuum bagging (an extension of the hand lay-up), vacuum bag resin infusion, resin transfer molding, filament winding, and pultrusion. Taking the nature of a composite structure into consideration, there are many combinations of materials and resins to choose from, therefore, the manufacturing process shall be selected according to the geometry of the part, its materials, and the available budget.

2.3.1 Hand lay-up

Out of all the manufacturing processes, the hand lay-up might be the most simple one and is compatible with any fiber or core material. As demonstrated in Figure 2.10, a mold with a gel coat or release agent is used to shape the fibers placed by hand on top of it, and resin is impregnated into the fibers with the help of a roller or a pencil. As it was emphasized,

before, this method is easy but does not let excessive resin be drained out of the part and no additional pressure or temperature is added in order to enhance mechanical properties during the curing process.

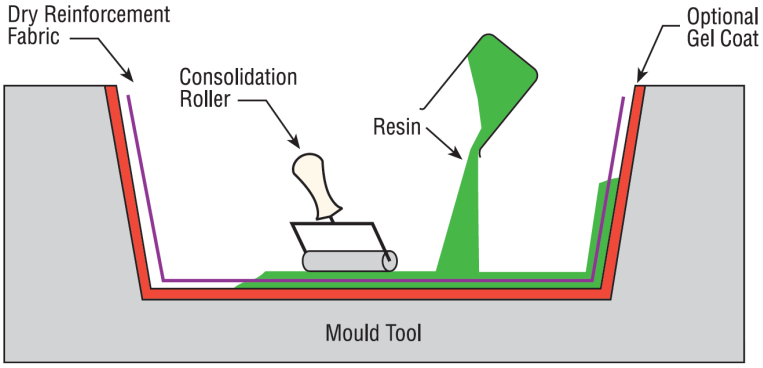

Figure 2.10: Schematic representation of the hand lay-up manufacturing process [22].

Advantages	Disadvantages
• Simple manufacturing process • Low cost of tooling materials • Compatible with a wide range of materials	• No resin excess extraction during the process • No compression on the part • Laminate quality is highly dependent on human factors

2.3.2 Vacuum bag hand lay-up

The Vacuum bag hand lay-up is a better version of the hand lay-up version and is also compatible with any fiber or core material. This manufacturing method can be used if one requires a part with less resin content and therefore, a higher specific strength. As demonstrated in Figure 2.11, the initial process is similar to the hand lay-up, but once the fibers are impregnated the vacuum equipment is placed on top of them. The vacuum equipment may include peel ply, which gives a rough surface finish to the part that can be useful for bonding, perforated film, that prevents the absorption film from sticking to the peel ply, a breather/absorption fabric, responsible for absorbing excess resin, vacuum bagging film, sealant tape and a vacuum pump (normally equipped with a vacuum gauge). Although this method is more expensive and labor-intensive than the hand lay-up, it provides substantially better composite parts where keeping the overall weight is of great importance.

Advantages	Disadvantages
• Excess resin can be removed from the part • Better fiber wet-out than the traditional hand lay-up • Compatible with a wide range of materials	• Extra cost added in labor and vacuum material • Higher lever of skill required by the operator • Laminate quality is still highly dependent on human factors

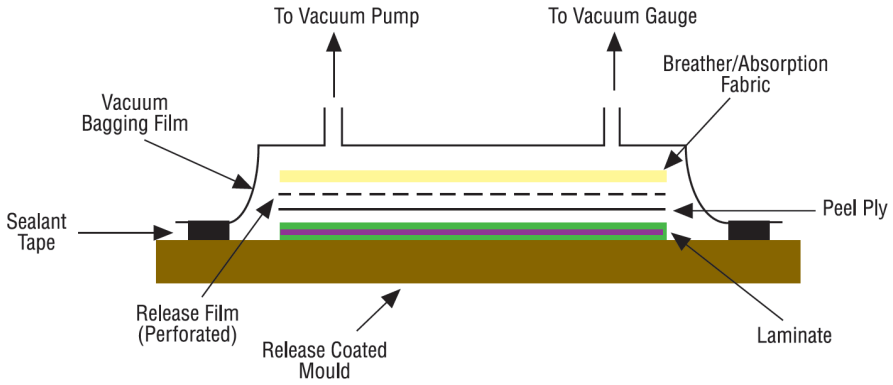

Figure 2.11: Schematic representation of the vacuum bag hand lay-up manufacturing process [22].

2.3.3 Vacuum bag resin infusion

Similarly to the vacuum bag hand lay-up, this process also relies on pressure, but in this version, the vacuum is used not only to compact the part but mostly to enable the resin flow into the dry stack up of fibers or core materials. As demonstrated in Figure 2.12 the materials are placed in the desired sequence on top of a previously prepared mold and, without any resin impregnation, the vacuum bag is closed. With the part now in a vacuum, the resin is introduced at one of its ends, which is then gradually ”pushed” through the fibers impregnating the same. In comparison with the hand laminating process, a higher volume of fiber can be achieved in the composite material. Although it is difficult to control the resin flow along edges and corners, higher fiber volume can be achieved in comparison to the hand lay-up method. It is also not possible to infuse honeycomb materials for a sandwich structure considering that the holes in the honeycomb would be filled with resin [23].

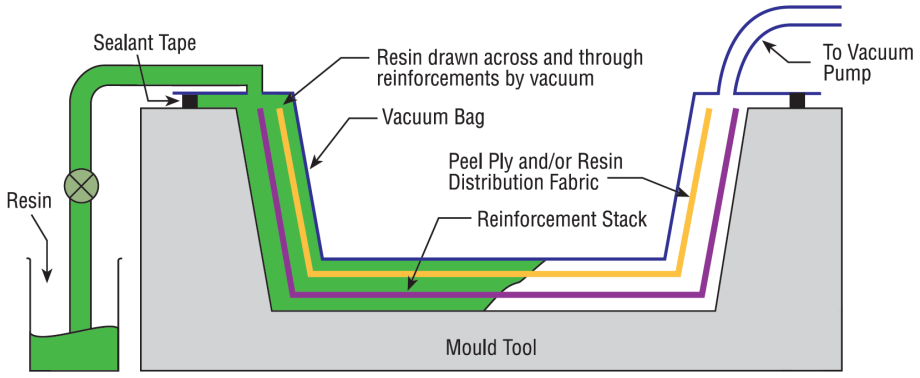

Figure 2.12: Schematic representation of the vacuum bagging resin infusion manufacturing process [22].

Advantages

- Lamination process is made in one go
- High fiber volume on the parts
- Lamination process less reliant on the operator

Disadvantages

- Incompatible with honeycomb cores
- Complex process
- Resins must be low viscosity

2.3.4 Filament winding

Filament winding is a manufacturing process primarily intended for convex-shaped components like pipes and tanks where continuous fiber tows are winded over a rotating or stationary mandrel. Figure 2.13 is a good example of a filament-winding process where the mandrel is rotating along its longitudinal axis. Continuous fiber tows pass through a resin bath and are deposited onto the rotating mandrel. Assuming that the mandrel is rotating at a constant speed, the orientation of the fibers is determined by the speed of the carriage moving parallel to the mandrel. Fiber tow orientation can range from 25° to 80° although 45° degree is the most common for stiffness and strength of convex parts [7].

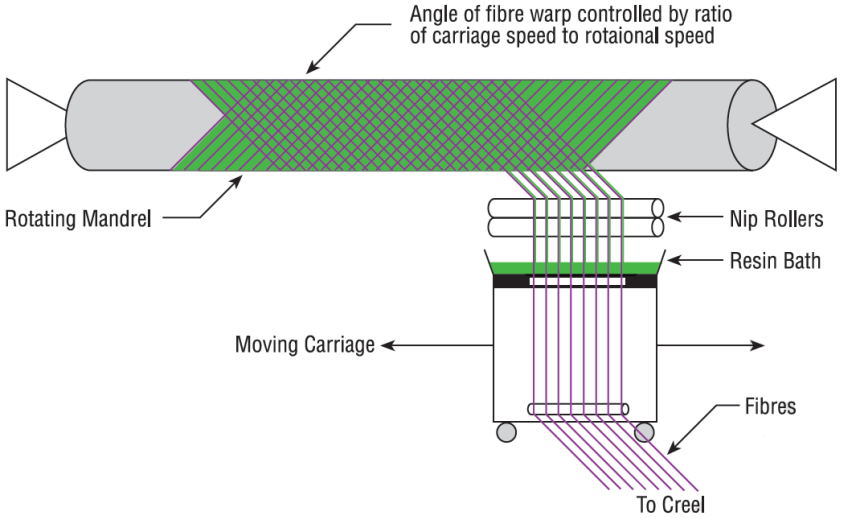

Figure 2.13: Schematic representation of the filament winding manufacturing process [22].

Advantages	Disadvantages
• Fast and automatized method • Reliable way to have straight and perfectly angled fibers • Using fibers makes it cheaper than buying cloth	• Fibers cannot be laid along the length of the part • Machinery is expensive • This process is limited to convex shaped components

2.3.5 Pultrusion

Pultrusion is a heavily automated laminating process designed to mass-produce parts with a constant cross-section (Figure 2.14). The process starts with the agglomerate of fiber tows that are positioned with the help of guides to accurately form the required cross-sectional shape and impregnate the fibers with resin. From this point, the impregnated fibers are pulled into the heated pultrusion die. The resin matrix is then solidified and cured within the die. The cured profile then lives the die and is automatically cut to length [24].

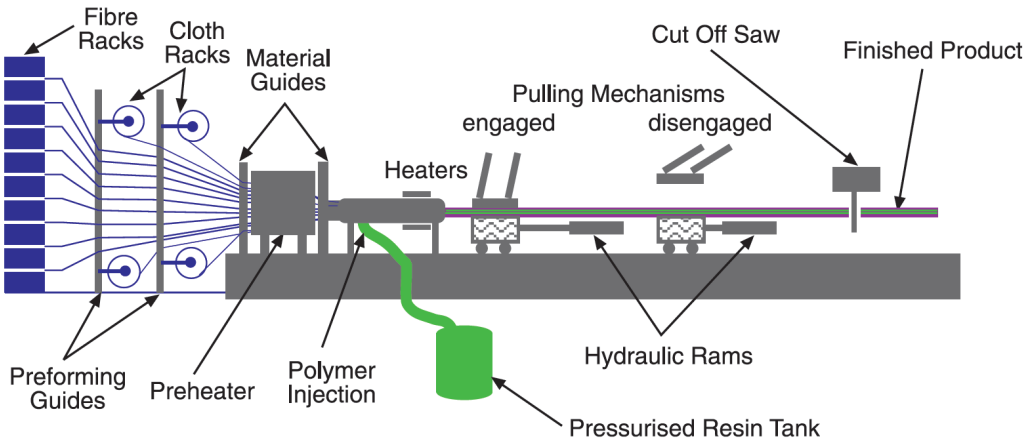

Figure 2.14: Schematic representation of the pultrusion manufacturing process [22].

Advantages	Disadvantages
• Fast and automatized method	• Limited to constant cross-section parts
• Resin content can be precisely controlled	• Heated die cost can be high
• Fiber tows are cheaper than fiber cloth	• Process not viable for non-production means

2.4 Failure modes of composite sandwiches

An important characteristic of a composite sandwich structure is that it is composed by two or more different material and evaluating the overall performance of this structures is not a simple task. It is difficult to tell just by the look of a composite sandwich structure how it will break or if it will fail either in the facings, the core or even the adhesive bonding between the two. Sandwich beams tested under general bending, in-plane loading or shear demonstrate various failure modes which can be visualized during testing and predicted by conducting stress analysis and applying failure criteria to the most critical section of the beam. For example, in a three point bending test configuration (Figure 2.15), most of the damage occurs in the middle of the beam where the force is being applied.

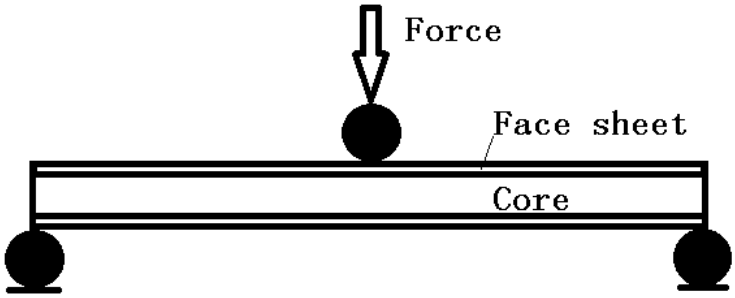

Figure 2.15: Simplified three point bending test configuration of a sandwich beam.

As described by [25], analyzing and predicting the failure mode of a sandwich structure can be especially demanding because of the inelastic and nonlinear behavior of some mate-

rials or even the interaction between failure modes. The most common failure modes may include face yielding due to tension, core shear or failure, indentation of the facing or core as a consequence of concentrated loads, debonding at the core/facing interface, wrinkling due to compression on the facing and buckling [26].

2.4.1 Face wrinkling

Face Wrinkling is a short wave length buckling phenomenon among many other possible buckling modes [27]. In a three point bending configuration the most evidences of face wrinkling are shown in the form of small wrinkles in the upper face of the sandwich structure where compression stresses are predominant (Figure 2.16).

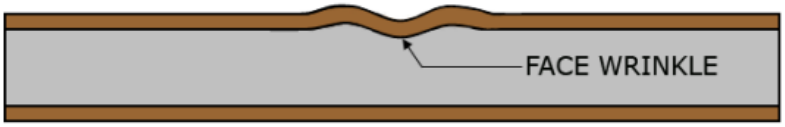

Figure 2.16: Face wrinkling of a composite sandwich due to compression of the upper face [28].

2.4.2 Face yielding

Failure due to face yielding of one of the faces occur when the axial stress reaches the in-plane failure stress of the face material [29]. Analyzing a composite sandwich as a beam under a bending stress equivalent to a three point bending configuration, it can be assumed that the stress in the compression face and tension face are the same. Composite materials have a lower compression strength and thus the face under compression is normally the critical one, although it is still possible for face yielding to occur on the lower face under tension (Figure 2.17).

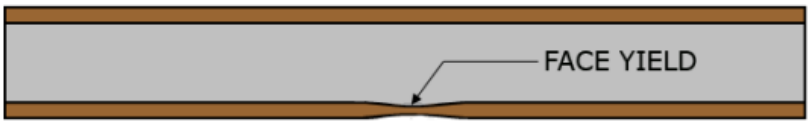

Figure 2.17: Face yielding of a composite sandwich due to tension on the lower face [28].

2.4.3 Core shear

Core shear can be visualized when the core of a sandwich structure is subjected to a shear stress greater than its core failure shear stress. As demonstrated in Figure 2.18 the shear stress is distributed through the face and core in a parabolic way having its higher value on the core section which can be explained by the most common low shear modulus of the core. If the faces are much stiffer and thinner than the core, which is true for most composite sandwiches, the shear stress can be simplified as linear along the faces and constant along the core [30]. Materials such as Nomex® honeycombs are particularly susceptible to core failure due to its anisotropic nature, in other words, its shear strength will depend on its orientation in relation to the loading. In Figure 2.19 the black rectangles represent

an approximate direction and location of cracks in a three point bending configuration of a composite sandwich.

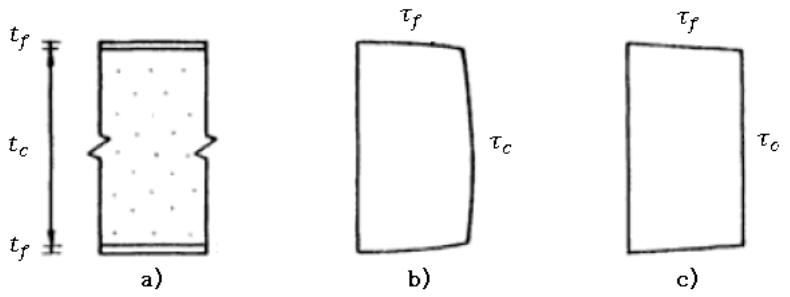

Figure 2.18: a) cross section of a composite sandwich, b) shear stress diagram of a composite sandwich c) simplified shear stress diagram of a composite sandwich (adapted from [30]).

Figure 2.19: Core shear on a composite sandwich (represented by the black rectangles) [28].

2.4.4 Indentation

Indentation occurs when the composite sandwich is subjected to a concentrated load which normally results in the crushing of an area under the loading point [31]. An indentation is normally not achieved on purpose but rather accidentally, for example, by a collision of a bird also known as a bird strike in the aviation industry. Indentation can also be the main failure mode when the facings of the composite sandwich are not strong enough to endure a localized load, or for example, in a honeycomb sandwich, if the load is only applied directly above one of the honeycomb holes, which therefore will only be supported by the facings. Figure 2.20 represents the indentation of a composite sandwich under a localized load.

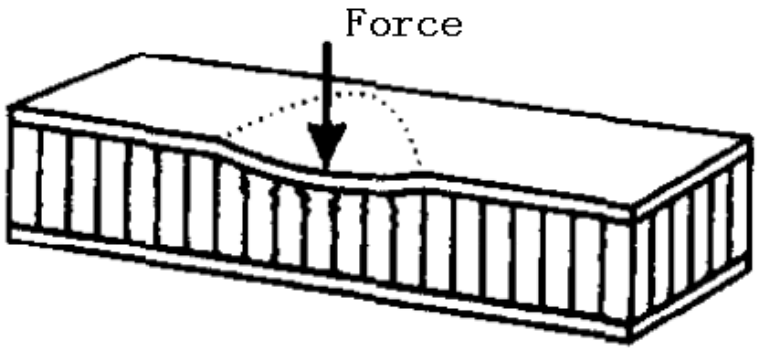

Figure 2.20: Indentation failure on a composite sandwich [29].

2.4.5 Debonding

Debonding is a failure mode that can occur when the bonding strength between the facings and the core is weaker than the shear strength of one of these materials (Figure 2.21). In a three point bending configuration, as the force is being applied, shear forces will be generated, and contrary to the core shear failure where the core material endures as much shear stress as possible until it fails, if the bonding between the facing and core is not strong enough, debonding failure will prevail. By separating the two materials, a debonding failure mode can be very unstable and brittle, and it can even cause an unexpected failure of the sandwich structure [32].

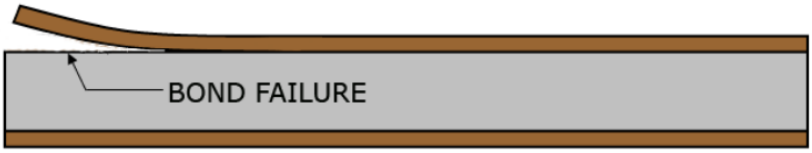

Figure 2.21: Debonding failure on a composite sandwich [28].

Chapter 3

Experimental procedure

This chapter describes the procedures used to conduct the experimental work and the guidelines followed to ensure valid results.

Section 3.1 - **Composite sandwich materials**, introduces the materials used in each sandwich composite sample and some of their elastic and mechanical properties.

Section 3.2 - **Standard test procedures and dimensions**, gives a summary of the content present in each standard used to test the specimens. Dimensions of the specimens and formulas to evaluate mechanical properties are also explored here.

Section 3.3 - **Production process**, explains the entire composite production process, from cutting the materials and laminating them into samples, to cutting the specimens into their dimensions.

3.1 Composite sandwich materials

With the main aim of getting a sandwich with the best performance, a variety of specimens were produced. Since most of glass fibers have a smaller specific strength than carbon fiber, all specimens will consist of only two carbon fiber sheets to strengthen each face of the sandwiches, with the used fabric having a surface mass of 30 g/m^2. For the core materials, balsa wood, AIREX® C 70.75 foam and Nomex® honeycomb were used, and for the matrix, a resin L and hardener EPH 500 were used in a ratio of 100:63 respectively.

Since these sandwich composite structures will be applied to small UAV wing skins, some characteristics are more desirable then others. These include having a high strength without compromising the weight of the structure, having a relatively small cross sectional thickness (below 3 millimeters) and being resistant to shear stresses.

The first sample is the reference composite sandwich, which is a widely used combination for UAV wing skins. This sample is composed of two carbon fiber sheets in each face (top and bottom), and a 1.7 mm thick and lightweight balsa wood core. For the second sample, a combination of two carbon fiber sheets in each face and a 2 mm thick AIREX® C 70.75 foam core were used. For the third and fourth samples, the same combination of two carbon fiber sheets in each face and a 2 mm thick Nomex® honeycomb core is used, being the main difference between one another, the orientation of the core represented as L (lengthwise) and W (widthwise), which as it will be seen, can lead to different results.

Table 3.1: Core material properties.

Properties	AIREX® C 70.75	Balsa wood	Nomex® honeycomb
$\rho\ [kg/m^3]$	80	120	30.56
$X_t\ [MPa]$	2	19.9	-
$X_c\ [MPa]$	1.45	6	0.9
$S\ [MPa]$	1.2	1.07	L: 0.5 W: 0.35
$E_1\ [MPa]$	66	1280	-
$E_2\ [MPa]$	66	19.2	-
$G\ [MPa]$	30	47.36	L: 25 W: 17
$\nu_{12}\ [-]$	0.100	0.488	-
$\nu_{23}\ [-]$	0.100	0.231	-

To comply with the shear stress resistance requirements, all of the samples were produced with two bidirectional carbon fiber sheets in each face (top and bottom), oriented at a 45º angle, since this is the orientation where the shear properties of the fibers are more predominant. This phenomena can be observed in Figure 3.1 by the increase of the shear modulus G_{xy} of a bidirectional carbon fiber fabric as it is rotated into a 45º orientation.

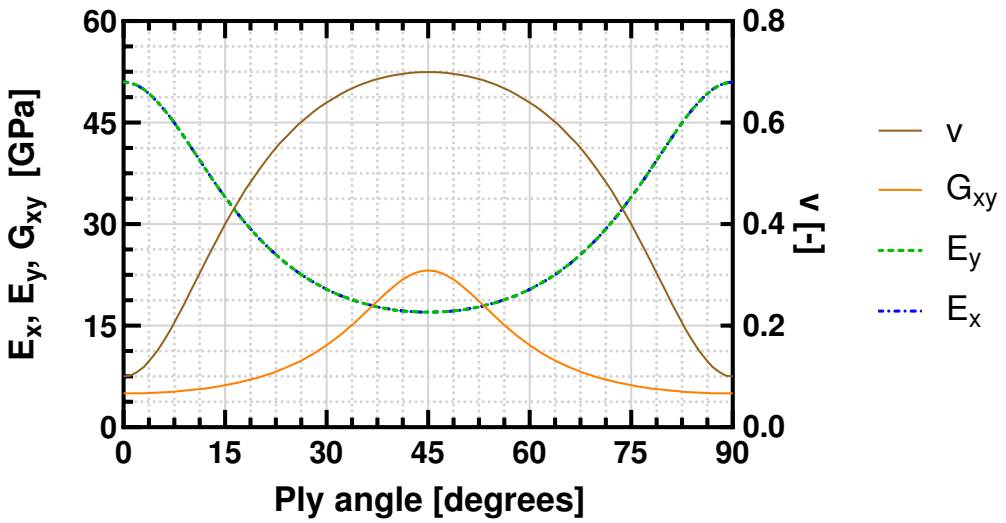

Figure 3.1: Bidirectional carbon fiber reinforced epoxy properties as a function of the ply orientation angle. Modulus of elasticity in the primary direction E_x, modulus of elasticity in the secondary direction E_y, shear modulus G_{xy} and Poisson ratio ν.

When compared to a unidirectional carbon fiber fabric, the bidirectional cloth has a better overall performance in all directions and can withstand loads applied in any direction. On the other hand, the unidirectional fabric has very high properties in the direction where its fibers are aligned with, but they start decreasing abruptly as it is tested in a 45º angle and having almost no resistance to any kinds of stress in a orthogonal direction (90º). This can be seen in Figure 3.2 where the modulus of elasticity in the primary direction is maximum at 0º (the direction of the fibers) and falls close to zero at 90º. The shear stress is significantly lower at a 45º angle when compared to a bidirectional cloth.

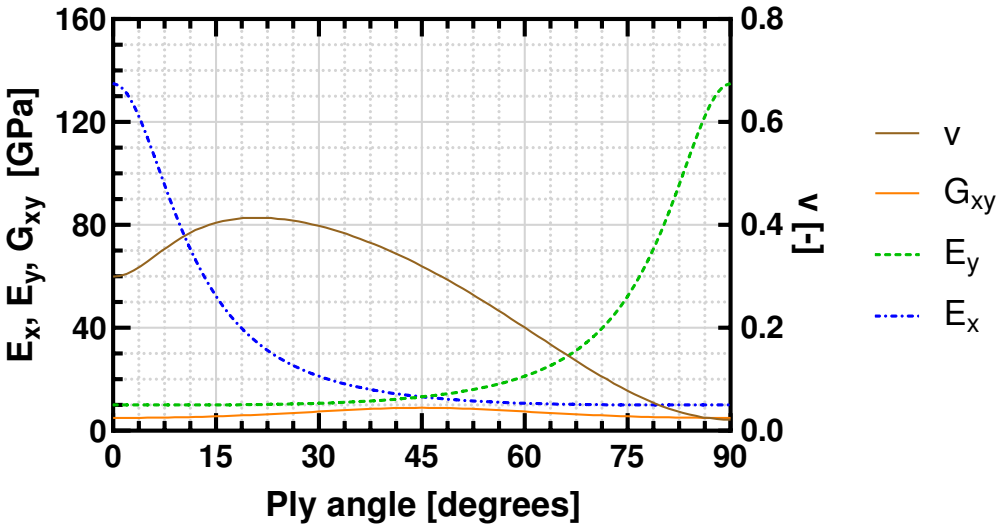

Figure 3.2: Unidirectional carbon fiber reinforced epoxy properties as a function of the ply orientation angle. Modulus of elasticity in the primary direction E_x, modulus of elasticity in the secondary direction E_y, shear modulus G_{xy} and Poisson ratio ν.

Other than the surface mass, no other data or additional information regarding the carbon fiber properties was provided by the manufacturer. The properties used in the simulations were the ones obtained in the work done by Santos et al. [33] and are shown in table 3.2.

Table 3.2: Bidirectional carbon fiber reinforced epoxy properties (adapted from Santos et al. [33]).

Properties	Woven carbon/epoxy
$\rho\ [kg/m^3]$	1600
$X_t\ [MPa]$	600
$X_c\ [MPa]$	540
$Y_t\ [MPa]$	600
$Y_c\ [MPa]$	540
$S\ [MPa]$	90
$E_1\ [GPa]$	51
$E_2\ [GPa]$	51
$G\ [GPa]$	5
$\nu_{12}\ [-]$	0.100
$\nu_{23}\ [-]$	0.100

3.2 Standard test procedures and dimensions

3.2.1 Equipment

The sandwich three-point bending tests were performed using a *Shimadzu AGS-X* Universal Testing Instrument (Figure 3.3), and although this machine can test materials with a pressing force of up to $50\ kN$, for this purpose, the loading cell was reduced to its lowest value of $500\ N$ to comply with the estimated theoretical maximum force applied in the center of the specimen which was lower than this value.

Figure 3.3: Shimadzu AGS-X Universal Testing Instrument.

The software *Trapezium X* was utilized to get an interface to directly watch the results from the tests, and also to capture important data, such as forces and deflections from the Universal Testing Instrument.

To calculate the fiber content of the specimens and their mass, a *Oertling VA204* high precision scale was also utilized.

3.2.2 Standard test methods

A certain degree of consistency is needed to compare the specimens' mechanical properties. To get this level of precision, organizations like the American Society of Testing Materials (ASTM) or the International Organization for Standardization (ISO) have standardized testing procedures and techniques. Flexural properties of composite sandwich structures are determined according to ATSM C393 and to determine the flexural properties of fiber-reinforced composites ISO 14125:1998 was utilized. Both standard test methods make use of a bending test performed in a universal testing instrument which, with the help of the *Trapezium X* software, will record a force (P) versus deflection (s) both measured in the middle of the beam.

A good way to analyze the final results of the bending test is to use the obtained data to curve a stress (σ) versus strain (ε) plot such as the one represented in Figure 3.4.

A simple value of the stress in the upper surface of the beam can be obtained by equation 3.1, and the strain by equation 3.2.

$$\sigma = \frac{3\,P\,l}{2\,b\,d^2} \quad (3.1)$$

where σ is the stress in the upper surface of the beam in $[MPa]$, P is the load applied on the

beam in $[N]$, l is the beam length in $[mm]$, b is the width of the beam in $[mm]$ and d is the thickness of the beam in $[mm]$.

$$\varepsilon = \frac{6\,s\,d}{L^2} \quad (3.2)$$

where ε is the strain in $[mm/mm]$ and s is the vertical displacement of the beam in $[mm]$.

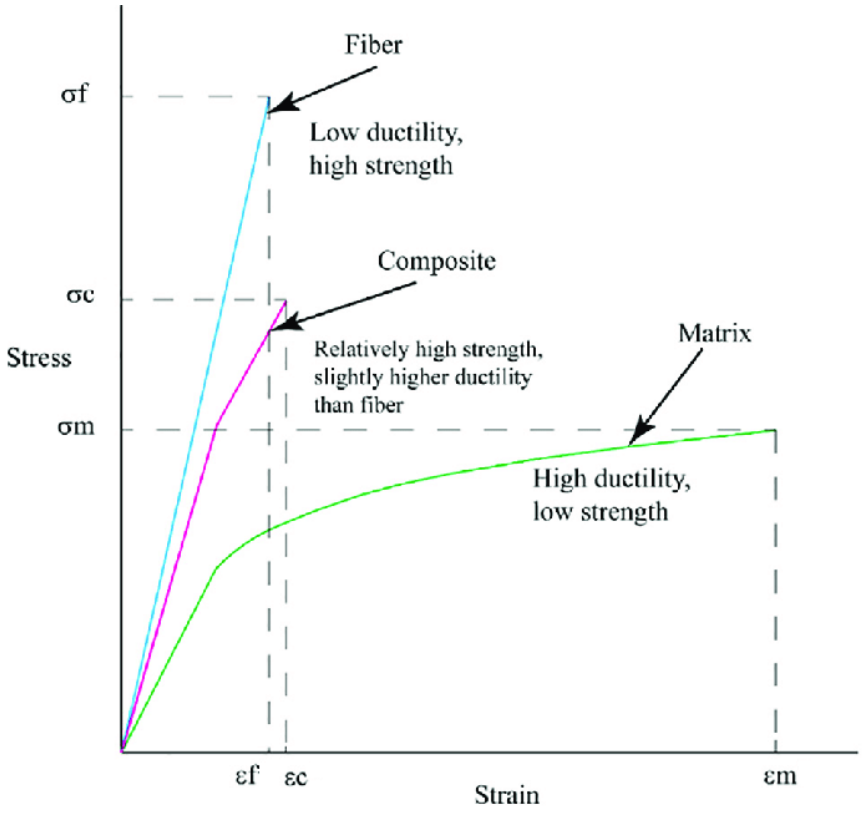

Figure 3.4: Schematic representation of a typical polymeric matrix composite stress-strain curve and its parts (fiber and matrix) [34].

Each material produces a different stress-strain diagram. The study of an individual material and its behavior from the point it is loaded until it breaks is of great importance to every engineer, and analyzing these charts can give critical information that enables a structure to have its future behavior a lot more predictable. Knowing the limits of each material also means being able to have lower safety margins, and consequently reducing weight, without the worry of a structural failure due to bad material properties characterization.

As the material is being loaded, both the stress and the strain increase proportionally until the yield strength is reached. The elastic limit of the material is reached at this point. This region is called the elastic zone of the material and its behavior can be described by Hooke's law (equation 3.3).

$$E = \frac{\sigma}{\varepsilon} \quad (3.3)$$

In Hooke's law, E $[MPa]$ is the modulus of elasticity, which is also known as Young's modulus. This constant represents the stiffness of the material, and the greater its value, the less a material elongates with a determined amount of stress. Ceramics, for example, have a very high modulus of elasticity which is reflected in their high bridle behavior.

In some cases this elastic region is not constant and therefore a tangent to the curve can be determined for a specific point. Alternatively, an average slope can also be calculated from two points with equation 3.4, where $\Delta\sigma$ and $\Delta\varepsilon$ are the difference in stress and strain, respectively, between the final point (ε_2, σ_2) and the initial point (ε_1, σ_1).

$$E = \frac{\Delta\sigma}{\Delta\varepsilon} = \frac{\sigma_2 - \sigma_1}{\varepsilon_2 - \varepsilon_1} \quad (3.4)$$

As the material continues being loaded after its yield strength, it enters the plastic zone and further elongation becomes irreversible. The ultimate strength is the maximum stress a material can endure without breaking and the fracture occurs when the material cannot support any more load, resulting in its failure.

3.2.2.1 Sandwich composite three-point bending test - ASTM C393

As stated before, ASTM C393 - "Standard test method for flexural properties of sandwich constructions" [35], was followed to ensure reliable results.

To comply with the standards and quote the article "the specimen shall be rectangular in cross-section. The depth of the specimen shall be equal to the thickness of the sandwich construction (*d*), and the width (*b*) shall be not less than twice the total thickness, not less than three times the dimension of a core cell (*c*), nor greater than one half the span length (*L*)" [35]. These dimensions are represented in the diagram of Figure 3.5 and the restrictions can be mathematically expressed as:

$$l \gg b \quad (3.5)$$

$$d = c + 2\,t \quad (3.6)$$

$$b \geq 2\,d \quad (3.7)$$

$$b \geq 3\,c \quad (3.8)$$

$$b \leq \frac{L}{2} \quad (3.9)$$

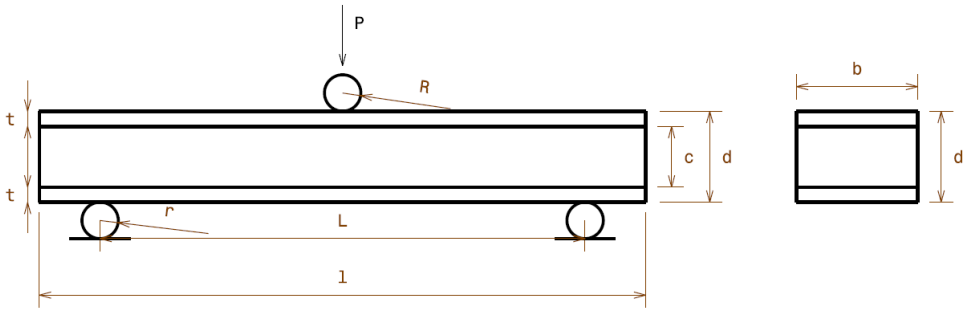

Figure 3.5: Front and side views of the three-point bending configuration for a composite sandwich.

In Figure 3.5, *P* is the applied load on the sandwich in $[N]$, *l* is the sandwich length in $[mm]$, *L* is the span length of the supports in $[mm]$, *t* is the thickness of the facings in $[mm]$, *c* is the thickness of the core in $[mm]$, *b* is the width of the sandwich structure in $[mm]$, *d* is the thickness of the sandwich structure in $[mm]$, *r* is the radius the lower supports in $[mm]$ and *R* is the radius of the upper support which is applying the load in $[mm]$.

Since the specimens have very thin layers of carbon we can simplify the restrictions and only account for the core thickness (*c*) to the total sandwich thickness (*d*).

The balsa wood core is 1.7 mm and both the AIREX® C 70.75 foam and the Nomex® honeycomb cores are $2\ mm$ thick. Following the restrictions, the sandwich width (*b*) for the $2\ mm$ thick cores shall have a dimension between $6\ mm$ and $50\ mm$ and between $5.1\ mm$ and $50\ mm$ for the balsa wood core. This way, it was opted to use $b = \ 25\ mm$ for all the specimens.

The projected dimensions of the specimens for each sandwich are given in Table 3.3 as follows:

Table 3.3: Projected dimensions for each specimen.

Variable	AIREX® C 70.75	Nomex® honeycomb	Balsa wood
$b\ [mm]$	25	25	25
$c\ [mm]$	2	2	1.7
$t\ [mm]$	0.06	0.06	0.06
$d\ [mm]$	2.06	2.06	1.76
$l\ [mm]$	130	130	130
$L\ [mm]$	100	100	100

A load should be applied to the specimen at a constant rate so that the maximum load occurs between 3 to 6 minutes from the start of the test. Based on rough estimations the appropriate cross-head loading rate z, must be $3\ mm/min$.

With the force and displacements recorded, the core shear stress and facing bending stress can be calculated with equations 3.10 and 3.11 respectively.

Core shear stress τ, in $[MPa]$:

$$\tau = \frac{P}{(d+c)\,b} \quad (3.10)$$

Facing bending stress σ, in $[MPa]$:

$$\sigma = \frac{P\,L}{2\,t\,(d+c)\,b} \quad (3.11)$$

Recalling equation 3.2, the flexural strain ε, of the upper carbon fiber layer can be obtained as follows:

$$\varepsilon = \frac{6\,s\,d}{L^2} \quad (3.2)$$

where *s* is the deflection recorded in the center of the sandwich beam in $[mm]$.

The bending modulus of elasticity of the sandwich structure (E_B), or flexural modulus of elasticity, can be calculated with equation 3.12.

$$E_B = \frac{L^3\,m}{4\,b\,d^3} \quad (3.12)$$

where L is the span length of the supports in $[mm]$, E_B is the bending modulus of elasticity in $[MPa]$, m is the slope of the tangent to the initial straight-line portion of the force-deflection curve in $[N/mm]$, b is the width of the sandwich structure in $[mm]$ and d is the thickness of the sandwich structure in $[mm]$.

To quantify the dispersion of the results and to examine if the data is reliable, a set of statistics may be evaluated. This include the sample mean (average) $\bar{x}$, the sample standard deviation S_{n-1}, and the sample coefficient of variation *CV*, shown in equations 3.13, 3.14 and 3.15 respectively [35].

$$\bar{x} = \left(\sum_{i=1}^{n} X_i\right)/n \quad (3.13)$$

$$S_{n-1} = \sqrt{\left(\sum_{i=1}^{n} x_i^2 - n\,\bar{x}^2\right)/(n-1)} \quad (3.14)$$

$$CV = \frac{100\ S_{n-1}}{\overline{x}} \quad (3.15)$$

where $\overline{x}$ is the sample mean (average), S_{n-1} is the sample standard deviation, *CV* is the sample coefficient of variation in [%], *n* is the number of tested specimens and *x* is the measured value of a single observation.

3.2.2.2 Carbon fiber laminate three-point bending test - ISO 14125:1998

To evaluate the carbon fiber laminate bending mechanical properties and ensure reliable results, the standard ISO 14125:1998 - "Fibre-reinforced plastic composites — Determination of flexural properties" [36] was followed.

This method is used to investigate the flexural behavior and to determinate properties such as the flexural modulus, flexural strength, flexural stress/strain curves, and deflections of the tested specimens. In this case, the carbon fiber specimens are manufactured from the same carbon fiber fabric of the sandwich tested with in section 3.2.2.1.

As for dimensions, the specimen shall comply with the ones given in the standard. These may vary depending on the bending test configuration (three-point or four point) or material. Table 3.4 is similar to the one given in the standard and represents the possible dimensions and tolerances for a three-point bending test. Since the the test revolves around a bidirectional carbon fiber composite material, the dimensions used were those from class IV. These dimensions are represented as variables in the diagram of Figure 3.6.

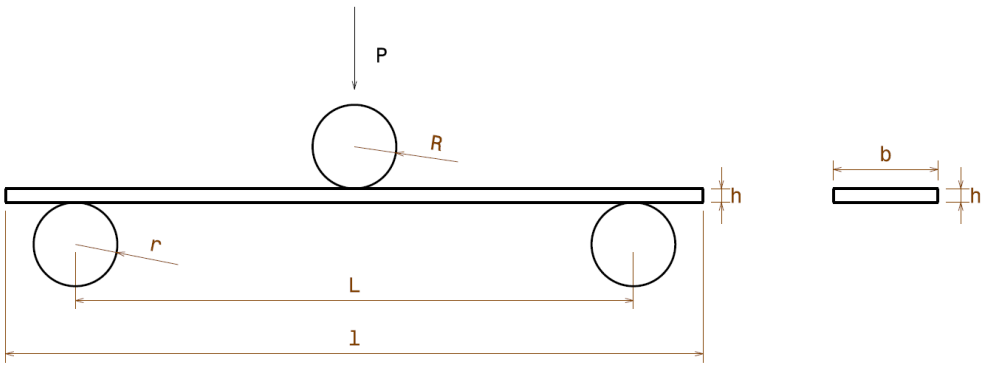

Figure 3.6: Front and side views of the three-point bending configuration for a fiber-reinforced beam.

In figure 3.6, *P* is the applied load on the sandwich in [N], *l* is the fiber-reinforced beam length in [mm], *L* is the span length of the supports in [mm], *h* is the thickness of the beam in [mm], *r* is the radius the lower supports in [mm] and *R* is the radius of the upper support

which is applying the load in $[mm]$.

Table 3.4: Three-point bending test projected dimensions for each material class. Class IV is highlighted and includes the dimensions used in the test (adapted from [36]).

Dimensions in millimetres

Material	**Specimen length** (l)	**Outer span** (L)	**Width** (b)	**Thickness** (h)
Class I Discontinuous-fibre-reinforced thermoplastics	80	64	10	4
Class II Plastics reinforced with mats, continuous matting and fabrics, as well as mixed formats. DMC, BMC, SMC and GMT.	80	64	15	4
Class III Transverse (90°) unidirectional composites; unidirectional (0°) and multidirectional composites. Glass-fiber systems.	60	40	15	2
Class IV Unidirectional (0°) and multidirectional composites. Carbon-fibre systems.	100	80	15	2
Tolerances	-0 / $+10$	± 1	± 0.5	± 0.2

The appropriate cross-head loading rate z, for a three-point bending test is given in the standard by the equation 3.16 where ε' is the strain rate of the material. In the absence of that information, the recommended value for the strain rate is $\varepsilon' = 0.01$.

$$z = \frac{\varepsilon' \, L^2}{6 \, h} \quad (3.16)$$

Replacing the variables with the appropriate values for this experiment the adequate cross-head loading rate comes as approximately $5.33 \; mm/min$.

After performing the three-point bending test, and with the collected force versus displacement data, the standard gives a method on how to determine the flexural stress, flexural modulus of elasticity and strain for the laminate.

For small deflections the flexural stress σ_f is given by the following equation:

$$\sigma_f = \frac{3 \, P \, L}{2 \, b \, h^2} \quad (3.17)$$

where σ_f is the flexural stress in $[MPa]$, P is the applied load in $[N]$, L is the span length of the supports in $[mm]$, h is the thickness of the specimen in $[mm]$ and b is the width of the specimen in $[mm]$.

In case deflections greater than $0.1L$ are observed, the flexural stress shall be calculated with Equation 3.18 as a way to correct larger-deflection effects.

$$\sigma_f = \frac{3\,P\,L}{2\,b\,h^2}\left[1 + 6\,\left(\frac{s}{L}\right)^2 - 3\,\left(\frac{s\,h}{L^2}\right)\right] \quad (3.18)$$

where s is the beam mid-point deflection in $[mm]$.

For the measurement of the flexural modulus, the deflections s' and s'' must be calculated with equations 3.19 and 3.20, where each deflection corresponds to the given values of flexural strain $\varepsilon'_f = 0.0005$ and $\varepsilon''_f = 0.0025$ respectively.

$$s' = \frac{\varepsilon'_f\,L^2}{4.7\,h} \quad (3.19)$$

$$s'' = \frac{\varepsilon''_f\,L^2}{4.7\,h} \quad (3.20)$$

where s' and s'' are the beam mid-point deflections in $[mm]$, ε'_f and ε''_f are the flexural strains, whose values are given above.

After getting the values of s' and s'' it is now necessary to extract the corresponding force values P' and P'' for the same displacements as shown in Figure 3.7.

The bending modulus of elasticity E_B, or flexural modulus of elasticity, can now be calculated from equation 3.21, which is an equivalent version of equation 3.12.

$$E_B = \frac{L^3}{4\,b\,h^3}\left(\frac{\Delta P}{\Delta s}\right) \quad (3.21)$$

where E_B is the flexural modulus of elasticity in $[MPa]$, Δs is the difference between deflections s'' and s' in $[mm]$, ΔP is the difference between forces P'' and P' at the deflection values of s'' and s' respectively in $[N]$.

Finally, for small deflections (smaller than $0.1L$) the strain in the outer surface of the specimen can be calculated as follows:

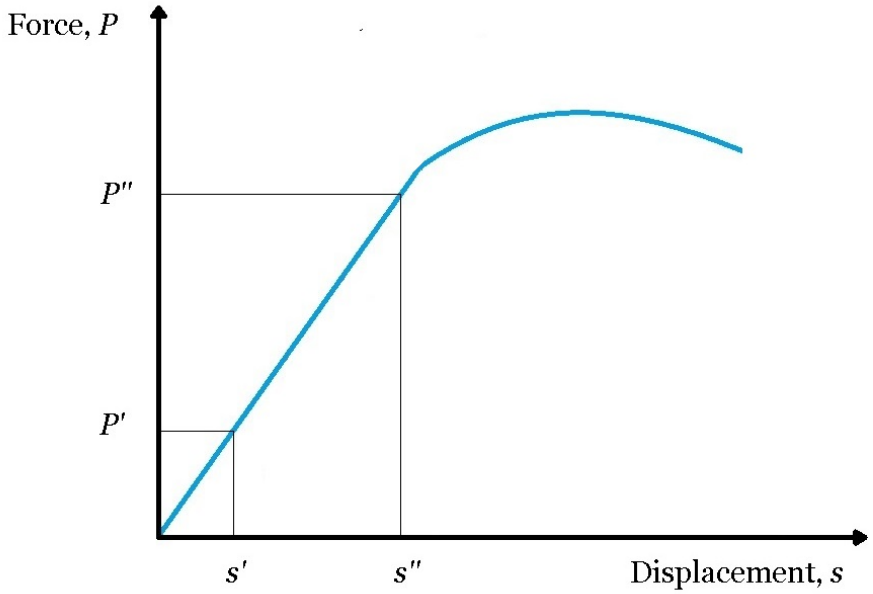

Figure 3.7: Schematic representation of the points (s', P') and (s'', P'') in a displacement versus force curve.

$$\varepsilon = \frac{6\, s\, h}{L^2} \quad (3.22)$$

where ε is strain in the outer surface of the specimen in $[mm/mm]$.

For deflections greater than $0.1L$ the strain in the outer surface of the specimen can be calculated as follows:

$$\varepsilon = \frac{h}{L}\left[6\,\frac{s}{L} - \left(\frac{s}{L}\right)^3 + 62.17\,\left(\frac{s}{L}\right)^5\right] \quad (3.23)$$

To quantify the dispersion of the results and to examine if the data is reliable, a set of statistics identical to the one described in the section 3.2.2.1 was used.

3.3 Production process

Each sandwich sample was produced separately but under the same conditions and only the Nomex® honeycomb sandwich had a different curing process and cutting technique that will be later described in this section. Each sample consists of a $270\ mm$ x $110\ mm$ sandwich that was cut in six identical specimens with $130\ mm$ x $25\ mm$.

Carbon fiber laminate specimens were also produced with a $100\ mm$ x $15\ mm$ rectangular shape and approximately $2\ mm$ thick.

3.3.1 Balsa and AIREX® composite sandwiches lay up

Starting with the balsa wood and carbon sandwich, the first step was to cut the materials for each set of specimens. Four rectangular sheets of carbon fiber with dimensions of $270\ mm$ x $110\ mm$ were cut on top of a hard surface with a roller cutter specifically designed to cut dry composite fiber, and since $30\ g/m^2$ is a thin fabric, it also gets very fragile, therefore, additional care was needed in the cutting process to not disturb the angle of each individual fiber. An aluminum ruler was also used to get a straight cut and only one but firm pass in one direction for each side of the rectangle was made with the roller to maintain the integrity of the fibers.

Balsa wood is considered an anisotropic material [37]. Nevertheless, to simplify engineering problems, it can be treated as an orthotropic material. The main idea to take away is that balsa wood is not isotropic and therefore, a careful consideration on the cut direction must be kept in mind. In this case a rectangle with dimensions of $270\ mm$ x $110\ mm$ was cut in the grain direction (Figure 3.8) for better performance. The cut was made in a flat surface with the aid of a razor blade and an aluminum ruler.

Figure 3.8: Balsa wood grain direction.

At this stage, and with the carbon fiber sheets and balsa wood cut, precise measurements of these material's mass were taken in a precision scale. By having the dry mass of these materials it is possible to measure the percentage of resin inside the sandwich composite after the curing process.

The next step consisted in cutting all the other necessary processing equipment. These included cutting a rectangle slightly bigger of peel ply fabric, perforated film, a non woven absorbent cloth and vacuum film. This vacuum film was then previously prepared with vacuum sealing tape and the vacuum hose was also plugged.

With all the materials ready, a glass surface was cleaned and brushed with release agent, which is responsible to make the composite sandwich not stick to the glass. After the release agent dried the resin mixture was prepared and the lay up process started. Firstly, enough resin was brushed on top of the glass surface to cover an entire $270\ mm$ x $110\ mm$ rectangle, then two carbon fiber sheets were laid up on top of the wet surface, one at a time. Right after, the resin covered balsa wood sheet was laid up followed by another two more carbon

fiber layer. To avoid excessive resin absorption of the balsa wood, just enough resin was used to guarantee that both the carbon fiber and balsa wood faces would get fully bonded. With no more resin usage at this stage, peel ply fabric, perforated film and non woven absorbent cloth were placed on top of the composite sandwich. The previously prepared vacuum film was then attached to the glass surface and the vacuum pump was turned on (Figure 3.9).

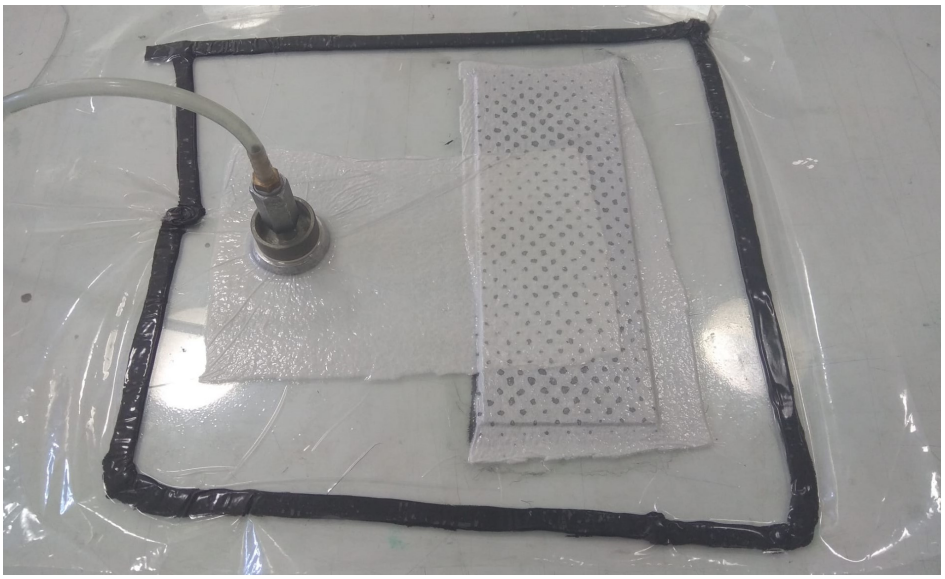

Figure 3.9: Vacuum bagging of the composite sandwich before curing.

For the AIREX® composite sandwich specimens, the production process was for the most part identical, being the only difference, the replacement of the $1.7\ mm$ balsa wood core by the $2\ mm$ AIREX® C 70.75 foam core.

3.3.2 Nomex® honeycomb composite sandwich lay up

Like the two samples described above, the Nomex® honeycomb composite sandwich has the same two layers of bidirectional carbon fiber with $30\ g/m^2$ in each side, and because the honeycomb structure has different properties in the lengthwise and widthwise directions, two separate samples were produced to evaluate any changes in performance.

One of the main features of this honeycomb structure is that it is composed of very thin 0.051 mm thick walls and hexagonal hollow spaces. Although this can create a very strong and lightweight core, it also comes with the downside of a low surface connection with the carbon fiber sheets and a lot of space to store non necessary resin inside each honeycomb, and therefore, excessive weight can be added to the sandwich. In Figure 3.10 the green lines represent the top or bottom faces of the honeycomb structure, which are consequently the bonding area between the core and carbon fiber faces.

To ensure that minimum weight was being added inside the hollow spaces, a good bonding between core and fibers was made, the lay up process was made in two separate curing cycles. Much like the balsa wood or the AIREX® foam sandwiches, the lay up process of the two first carbon fiber layers was identical, but in this case, after adding the $2mm$ thick

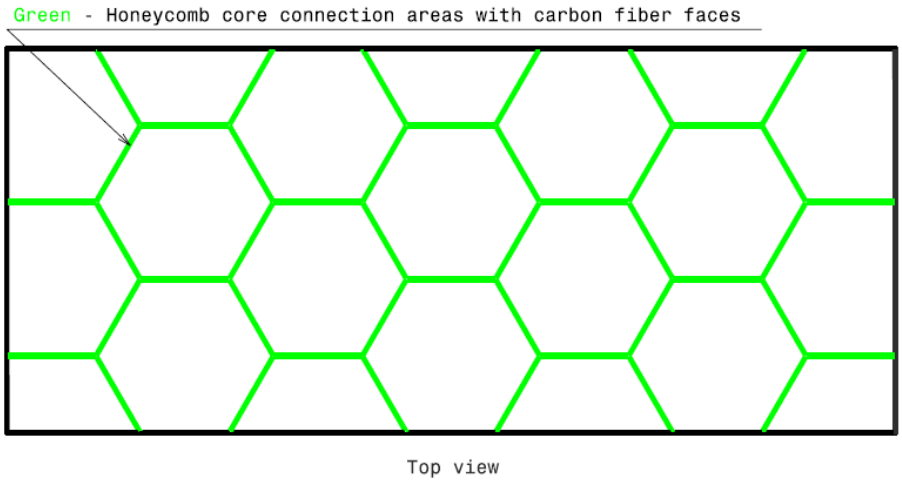

Figure 3.10: Honeycomb bonding lines with the carbon fiber faces represented by the green areas.

Nomex® honeycomb core, the vacuum bag was closed and the sample was let to cure. After this curing was completed, the sample was removed from the glass surface, which had to be cleaned and prepared to laminate two more carbon fiber layers, and then, the previously cured, but not finished sample, was turned upside down (carbon fiber layers facing up) and the honeycomb core was placed on top of the two newly laminated carbon fiber layers. Finally the vacuum bag was closed once again and another curing cycle was made for the sample.

3.3.3 Carbon fiber composite lay up

In order to comply with ISO 14125:1998 the specimens were required to have 100 mm in span, $15\ mm$ in width and $2\ mm$ in thickness. Although getting the span and the width with the correct dimensions was simple, getting the required thickness with a $\pm\ 0.2\ mm$ was not so straightforward. To solve that problem, the theoretical number of layers needed to achieve a $2\ mm$ laminate was calculated.

For a single cured ply its thickness t_{ply}, is given by the following equation:

$$t_{ply} = \frac{\gamma_f}{1000\ \rho_f\ V_f} \quad (3.24)$$

where t_{ply} is the thickness of a single cured ply in [mm], γ_f is the fiber surface mass in [g/m^2], ρ_f is the density of the fibers in [g/cm^3] and V_f is the fiber volume fraction.

The fiber volume fractions may vary depending on the experience of the operator who lays up the composite but it is mainly dependent in its laminating process. Table 3.5 gives typical values for different types of laminating processes estimated from R&G Composite [38], a recognized German composite distributor:

Table 3.5: Typical values of fiber volume fraction V_f, for hand lay-up, vacuum bagging and vacuum resin infusion laminating processes provided by R&G Composite.

Laminating process	Hand lay-up	Vacuum bagging	Vacuum resin infusion
Fiber volume fraction, V_f	0.35	0.40	0.5

In this case, the process was performed with a vacuum bagging technique, but since the values in Table 3.5 assume that no void spaces (areas without resin or with air) are created inside the laminate, it was experimentally observed that the fiber volume fraction had a value of $V_f = 0.375$ or in other words, the laminate had $37.5\ \%$ of its volume in fibers when laminated with the vacuum bagging technique under the laboratory conditions.

For the other variables, the fiber area weight is $\gamma_f = 30\ g/m^2$ and the density of the fibers was assumed as a regular carbon fiber material with $\rho_f = 1.77\ g/cm^3$.

Arranging equation 3.24 with the new values, the thickness of a single cured ply comes as $t_{ply} = 0.0452\ mm$.

To get the required number of layers it is only needed to divide the desired layer thickness h, by the previously obtained cured ply thickness t_{ply}, as shown by equation 3.25.

$$n_{plies} = \frac{h}{t_{ply}} = \frac{2}{0.0452} \approx 44\ plies \quad (3.25)$$

where n_{plies} is the number of plies in the cured laminate and h is the desired laminate thickness in [mm].

Because of the amount of plies needed and to reduce the amount of carbon fiber used, it was decided that only two specimens were produced instead of the five required by the standard, and although this is a low number of specimens, maximum precision was taken into account to ensure precise results.

The required layers could now be cut in rectangular shapes with enough size for two specimens and a slight margin in the dimensions to account for the post processing phase. The laminating process was similar to the ones described before for the sandwich specimens, with the only difference being that there was no core material , but instead, only carbon fiber plies stacked one-by-one with enough resin to impregnate all layers.

Since this lay up was made in the winter season, the specimens were subjected to additional heat during the curing phase to account for the low temperatures in the laboratory.

Figure 3.11: Carbon fiber laminate sample after the lay up process (before cutting).

3.3.4 Post processing

With each sample cured, guiding lines were marked on top of the 270 mm x 110 mm samples and from each sample, six specimens were cut in identical 130 mm x 25 mm smaller rectangles, as shown in the sketch of Figure 3.12, with a radial saw table. To get the right dimensions, some extra hand sanding was also needed on each edge of the specimens.

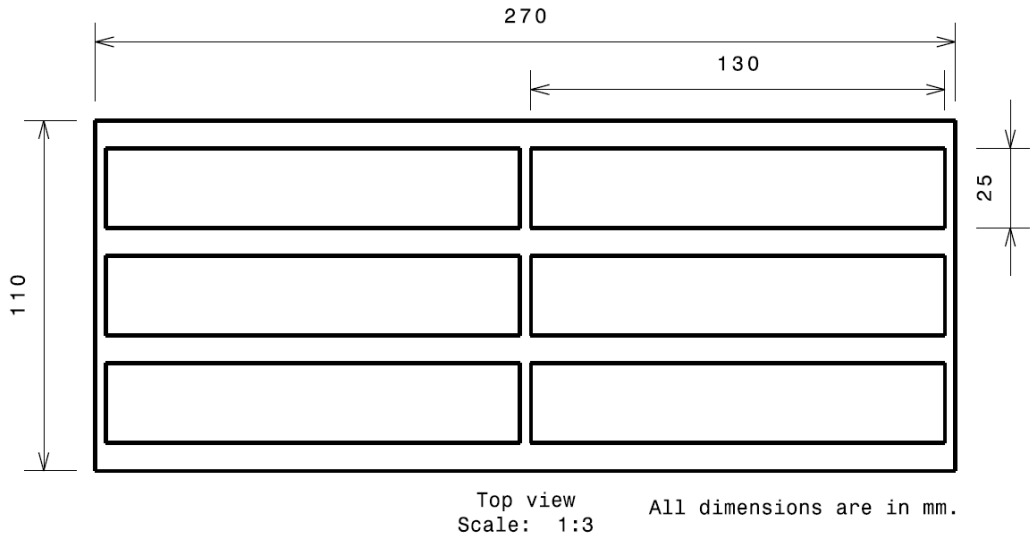

Figure 3.12: Composite sandwich sample cutting sketch.

In Figure 3.13 a), b), c) and d), it is possible to get a closer look at the final appearance of the balsa wood sandwich, the AIREX® C 70.75 foam core sandwich, the Nomex® honeycomb core sandwich in the lengthwise direction and the Nomex® honeycomb core sandwich in the widthwise direction respectively.

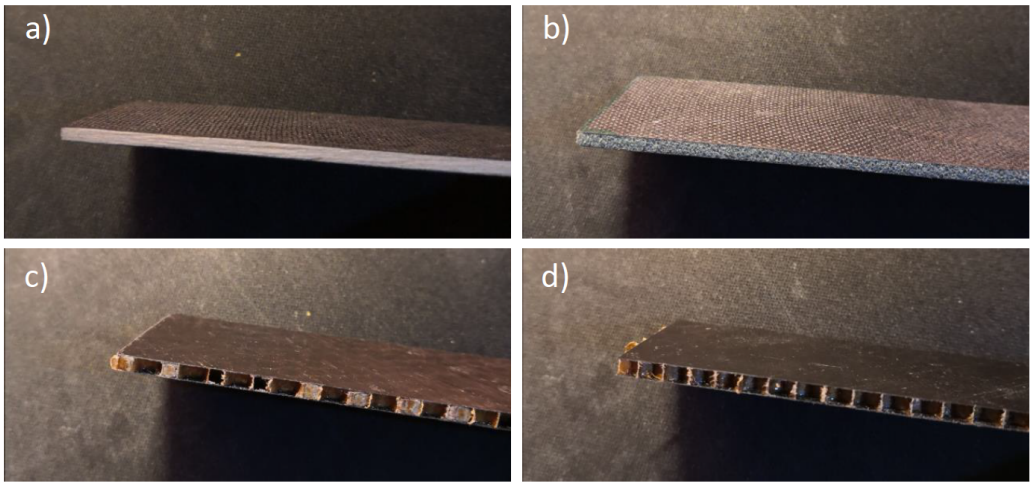

Figure 3.13: Final appearance of a specimen from each sandwich sample. a) Balsa wood sandwich, b) AIREX® C 70.75 foam core sandwich, c) Nomex® honeycomb core sandwich in the lengthwise direction and d) Nomex® honeycomb core sandwich in the widthwise direction.

Similarly to the sandwich samples, the carbon laminate sample was also marked with the specimen dimensions ($100\ mm$ x $15\ mm$), cut with a radial saw and sanded to the right dimensions. The two specimens can be seen in Figure 3.14.

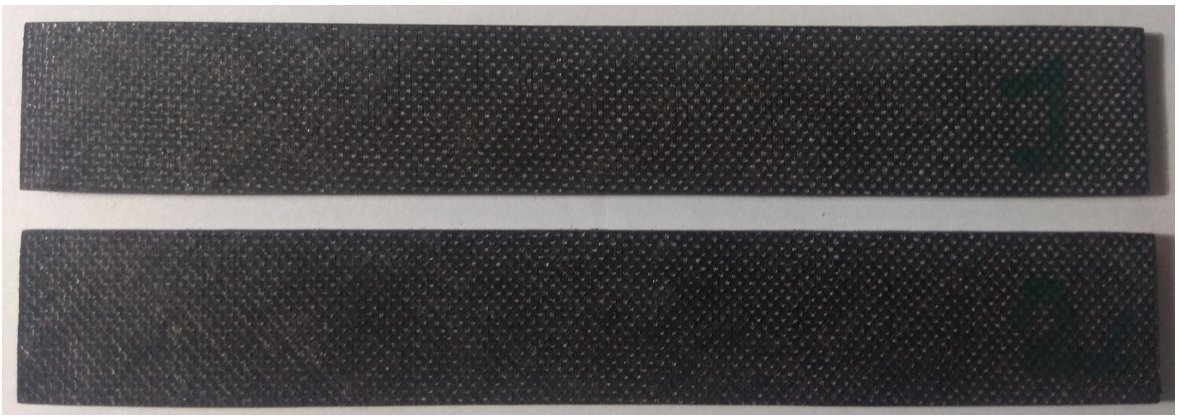

Figure 3.14: Carbon fiber laminate sample after the cutting process cutting.

Chapter 4

Finite element analysis

This chapter aims to give a brief explanation of what are a Finite element analysis and the main features needed to take into account when performing one. The steps and techniques used to run the simulation are also described throughout this chapter.

This chapter is divided into six sections.

Section 4.1 - **FEA definition**, gives a definition of what a finite element analysis is and what its main purpose is.

Section 4.2 - **Methodology**, explains the tools and processes needed to run the FEA.

Section 4.3 - **Geometry**, describes the geometry creation process.

Section 4.4 - **Materials definition**, describes which materials are used in the analysis and how are these defined in the software.

Section 4.5 - **Meshing and composite definition**, summarizes the main aspects behind the meshing of the geometry and the definition of the composite sandwich structure.

Section 4.6 - **Boundary conditions**, describes how some features like the boundary conditions, dedicated named selections, displacements, and supports were defined.

4.1 FEA definition

Finite element analysis (FEA) is the process of modeling and analyzing systems or structures in a virtual environment using the finite element method. A finite element model (FE) consists of a system of points called ”nodes” that form the shape of the design. Connected to these nodes are the finite elements themselves that make up the finite element mesh and contain the model’s material and structural properties that define how the model responds to certain conditions [39].

Knowing how to use FEA and extract the required data from this analysis is very important in many engineering fields since it can reduce the number of prototypes created while also optimizing a certain system by predicting and improving its performance and reliability, being able to evaluate different designs and materials, and reducing weight.

4.2 Methodology

A 2021 version of ANSYS® workbench software was used to run all the analysis steps, including the materials definition, meshing, composite pre-processing, and mechanical evaluation as shown in Figure 4.1. The geometry was drawn in a CAD (computer-aided design) drawing dedicated software.

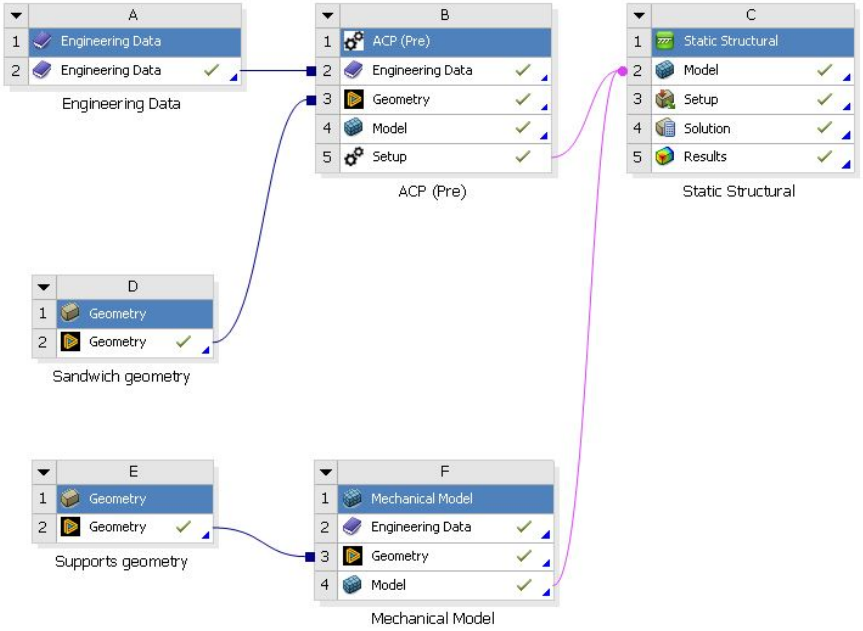

Figure 4.1: Representation of the ANSYS® workbench scheme.

The first step of the analysis starts by using the CAD software to draw the geometry, in this case, the entire three-point bending test configuration, including the supports and the sandwich structure. After that, the geometry can be imported to ANSYS® workbench where the predetermined materials are going to be assigned to the corresponding geometries. A specific component system of ANSYS® workbench named ”ACP (Pre)” was used to organize each ply of the composite structure and after having the meshed geometry, the static structural analysis system (also inside ANSYS® workbench) was used to define the boundary conditions, contacts, loads or displacements, and ultimately the results from the analysis.

4.3 Geometry

As stated before, the geometry was entirely drawn with the CAD software. The geometry was drawn in different bodies as entire solids and, depending on the specimen being analyzed, necessary changes were made to the dimensions of the geometry.

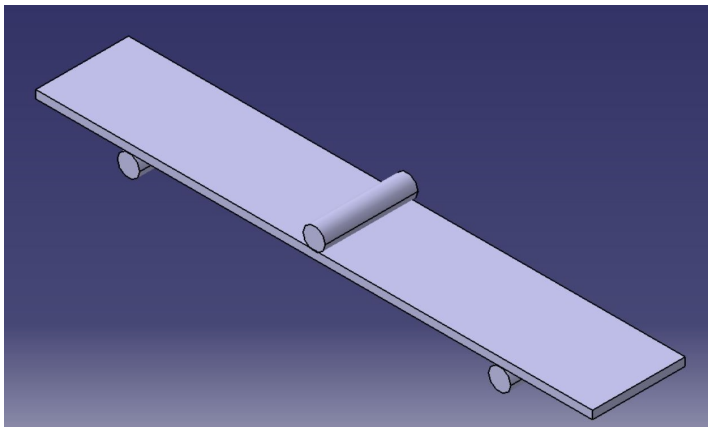

Figure 4.2: Three-point bending configuration geometry designed in the CAD software.

4.4 Materials definition

The materials used for each sandwich structure were defined with the same properties as already described in the Tables 3.1 and 3.2.

Both carbon fiber and balsa wood were defined as orthotropic materials due to the nature of their direction-dependent properties and the other core materials were defined as isotropic homogeneous core materials.

4.5 Meshing and composite definition

For this study, hexahedral elements with eight nodes per element were used to define the mesh. Although the model is simple, the boundary conditions of this study make the simulation very hardware demanding especially for the computer's RAM and therefore, it was decided not to make a great refinement in the sandwich mesh. This mesh can be seen in Figure 4.3 where a mesh quality of 1 represents a perfectly regular element, in the chosen quality measure, and 0 represents a degenerated element. Finally, the model has a total of 2799 elements and 4937 node.

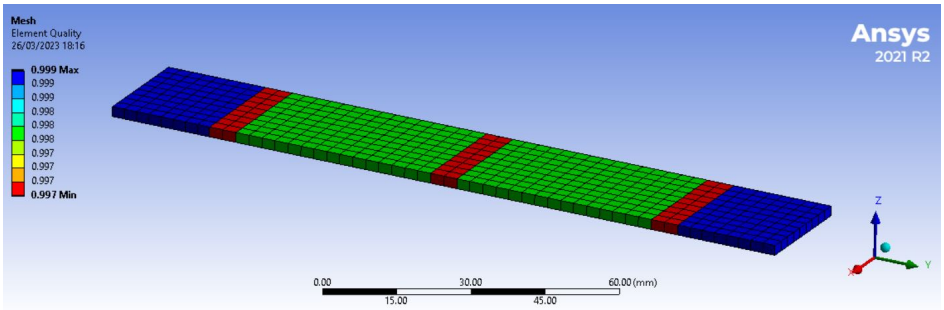

Figure 4.3: Mesh used for the sandwich geometry and quality of each individual element.

The stacking order and orientation of the elements in the composite sandwich structures were defined in the "ACP (Pre)" component system within ANSYS® workbench.

The carbon fiber ply (Figure 4.4) was defined with the material properties from Table 3.2 and a thickness of $0.0452\,mm$ which is the same as the one obtained with equation 3.24.

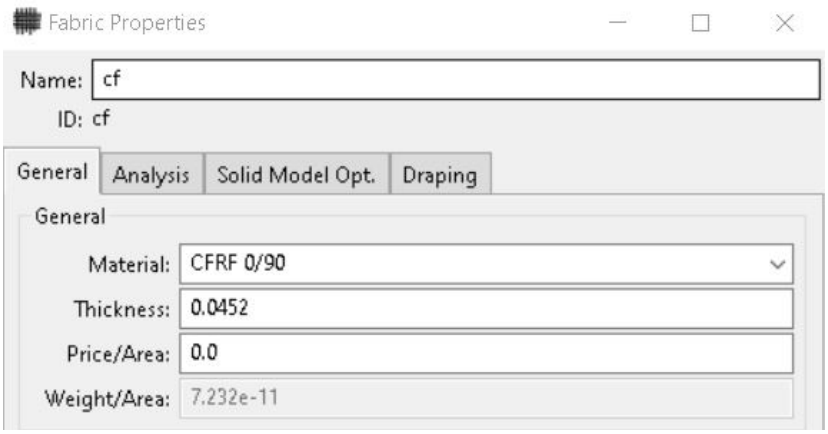

Figure 4.4: Definition of a single carbon fiber ply in ACP (Pre).

A rosette was also created in order to define the principal and orthogonal directions of the composite structure. This rosette has its primary axis (represented in Figure 4.5 as the x axis) aligned longitudinally with the sandwich's span and the secondary axis perpendicularly oriented to the primary axis.

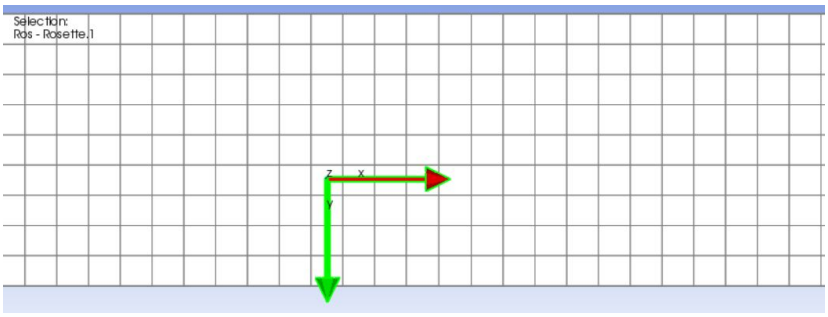

Figure 4.5: Rosette used to define the principal and orthogonal direction of the composite structure.

As described previously in this document, the carbon fiber layers had to be aligned in $\pm$ 45º angle with the span of the specimen. The same can be seen in Figure 4.6.

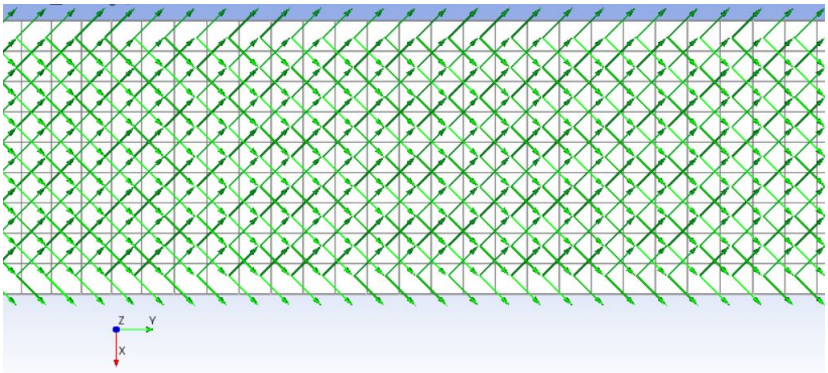

Figure 4.6: Fiber direction of the carbon fiber epoxy fabric in the sandwich model.

4.6 Boundary conditions

The last step before running the simulation is to set up the boundary conditions which include the connections between the sandwich structure and the supports, and the displacements to all the supports.

In order to simulate the experimental scenario in which the specimens were tested, an important feature to take into account is the type of contact between each face. By default, the connections are set as bonded but, unfortunately, these are not adequate to this study, since in a real-life scenario the faces of the sandwich structure are not bonded to the supports. They are frictionless, or at most, frictional with a small friction coefficient which means that the facings of the sandwich structure are able to slide upon experiencing bending duo to the applied load. Otherwise, stretch-induced stress would be created in the bonded facings resulting in a premature failure of the structure.

Three dedicated sections, which are represented in Figure 4.7 as the target bodies (blue faces) of the composite sandwich, were created to take into account the contact between the supports and the sandwich facings. The load support (Figure 4.7-a) is set as frictional with a friction coefficient equal to 0.1 and both the left and right supports are set as frictionless (Figure 4.7-b).

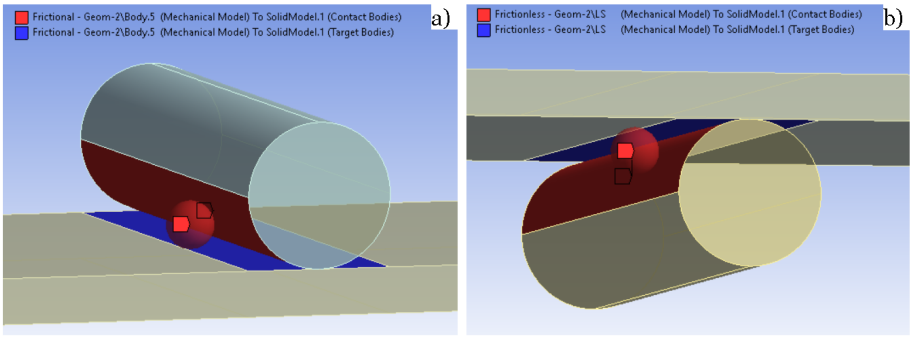

Figure 4.7: Contact definition between the supports and the sandwich facings. a) Load support connection (frictional), b) Left and right support connection (frictionless).

In order to constrain the geometry, all the supports were assigned a remote displacement. For the load support (Figure 4.8 A) the displacement was only allowed in the z direction and all the other translations were fixed for the remaining directions. The bottom supports (Figure 4.8 B and C) had their displacements constrained from any translation in any direction, making this two, a pair of fixed supports.

Although the objective of this simulation was to subject the composite sandwich to a force and return the deflection, the opposite was made in order to get convergence in the simulation. For that, a range of tabulated values of deflection (negative values because the direction is opposite to the z axis) were attributed to the load support, and a force probe (Figure 4.9) was placed in each bottom support making the sum of both, the reaction force of the load support acting on the composite sandwich.

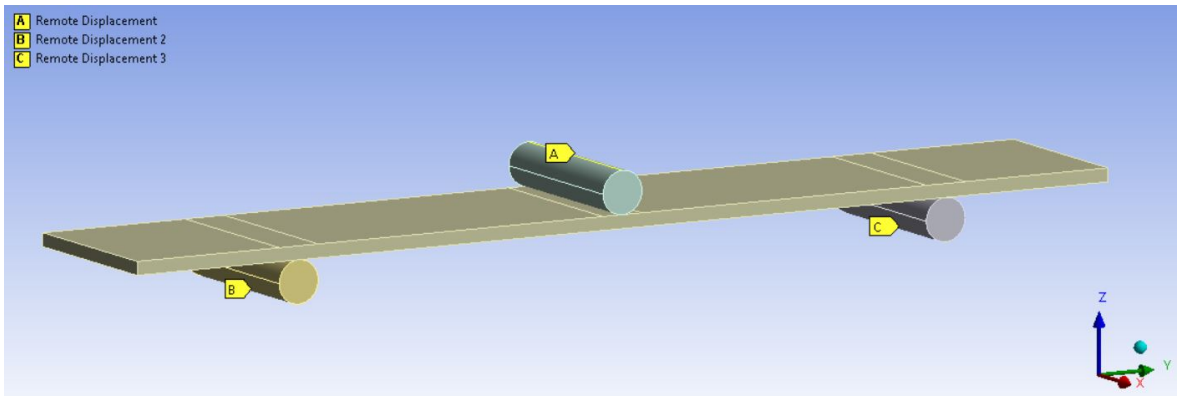

Figure 4.8: Boundary conditions of each support. A- Only allowed to move in the negative z direction with no rotation, B and C - Not allowed to move or rotate in any direction.

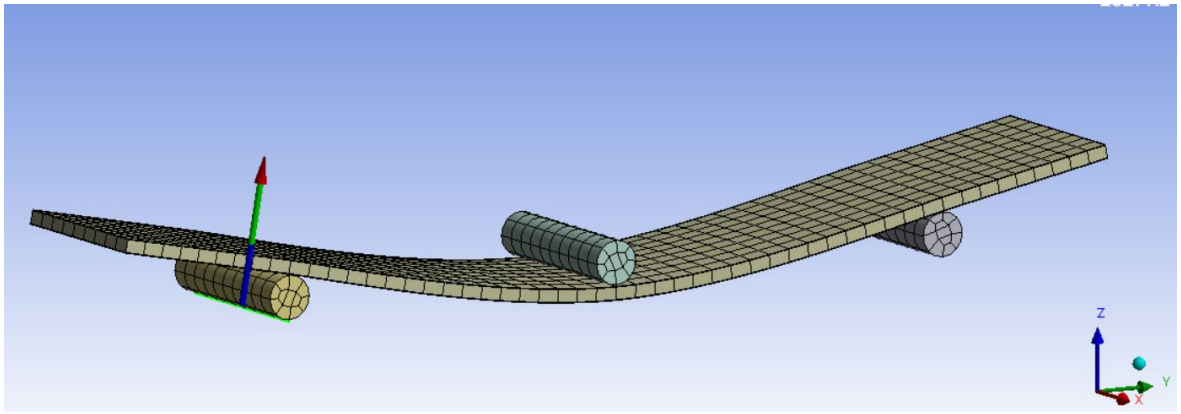

Figure 4.9: Reaction force on the left support.

The last step was to get the deformation (Figure 4.10), normal stress on the top layer of the sandwich structure and the shear stress for the core material.

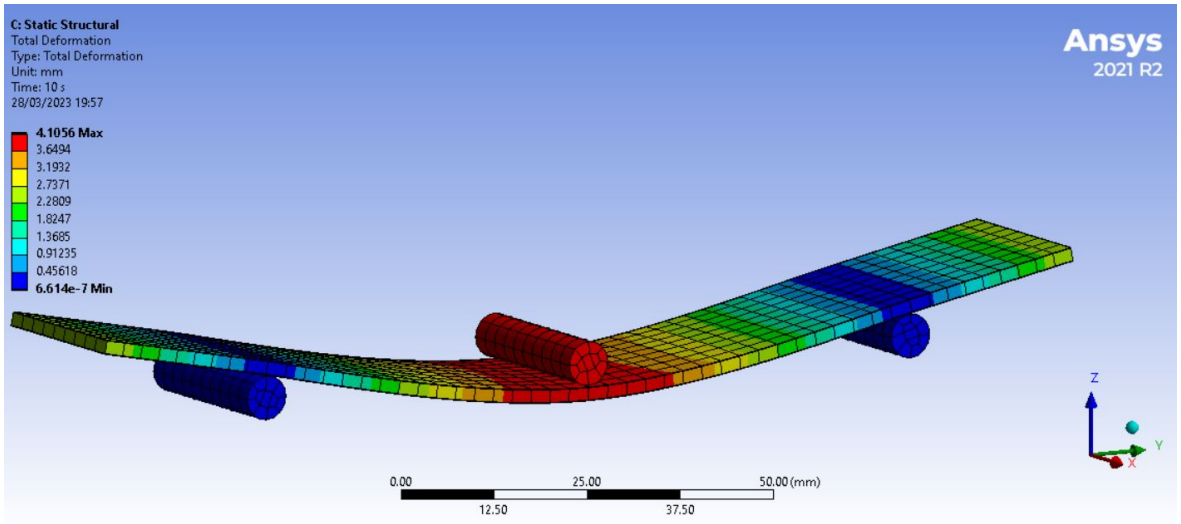

Figure 4.10: Deformation results from ANSYS®.

Chapter 5

Results

Figure 5.1 shows the failure mark of each composite sandwich sample highlighted in red, with each sample accordingly labeled, being a) Balsa Sandwich, b) AIREX® sandwich, c) Nomex® honeycomb lengthwise sandwich and d) Nomex® honeycomb widthwise sandwich.

All the sandwich samples had their failure in the carbon fiber facings. Both samples a) and b) have failed due to face wrinkling, and although samples c) and d) also failed from wrinkling, it is visible that the crack propagated more irregularly by following the hollow spaces from the honeycomb core where there is no support for the facings.

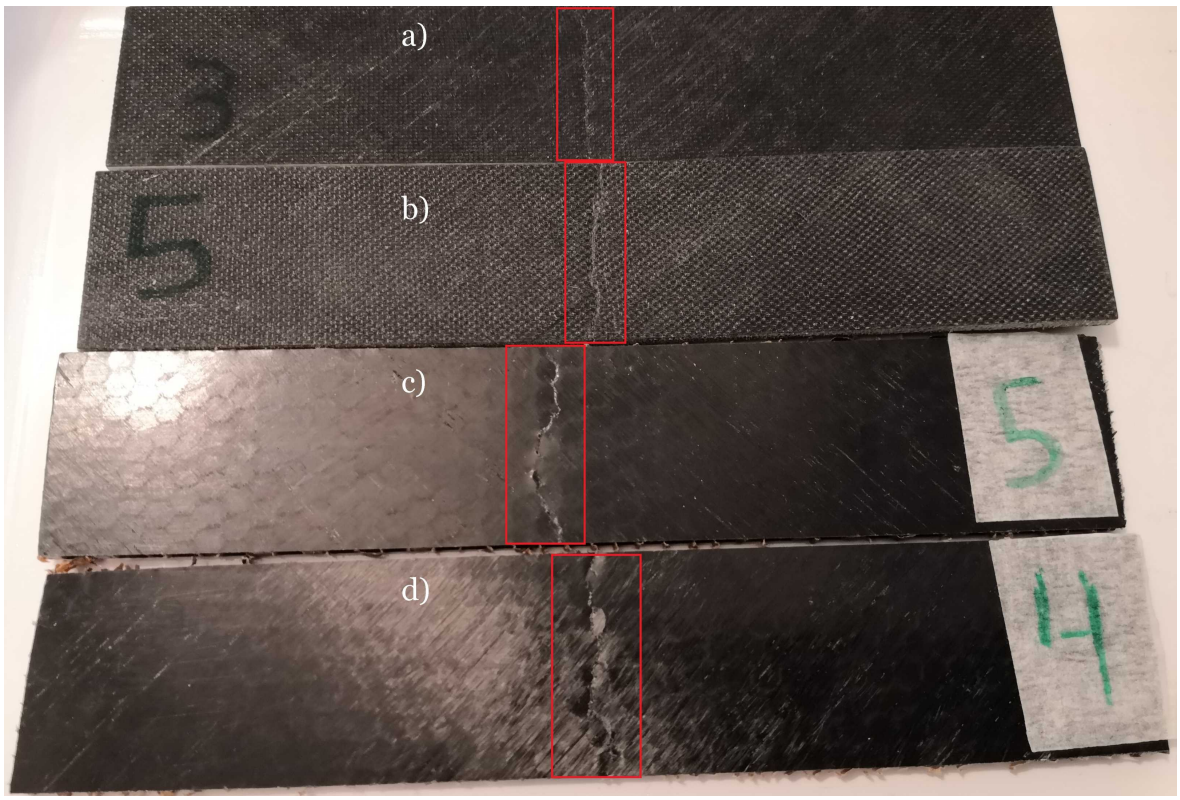

Figure 5.1: Failure of the carbon facings in each sandwich specimen. a) Balsa Sandwich, b) AIREX® sandwich, c) Nomex® honeycomb lengthwise sandwich and d) Nomex® honeycomb widthwise sandwich.

Represented in Figure 5.2 are the three-point bending test charts for each set of specimens, where the displacement s, is represented in the x axis, and the load applied P is represented in the y axis. The individual test of each specimen can be found in Appendix A.

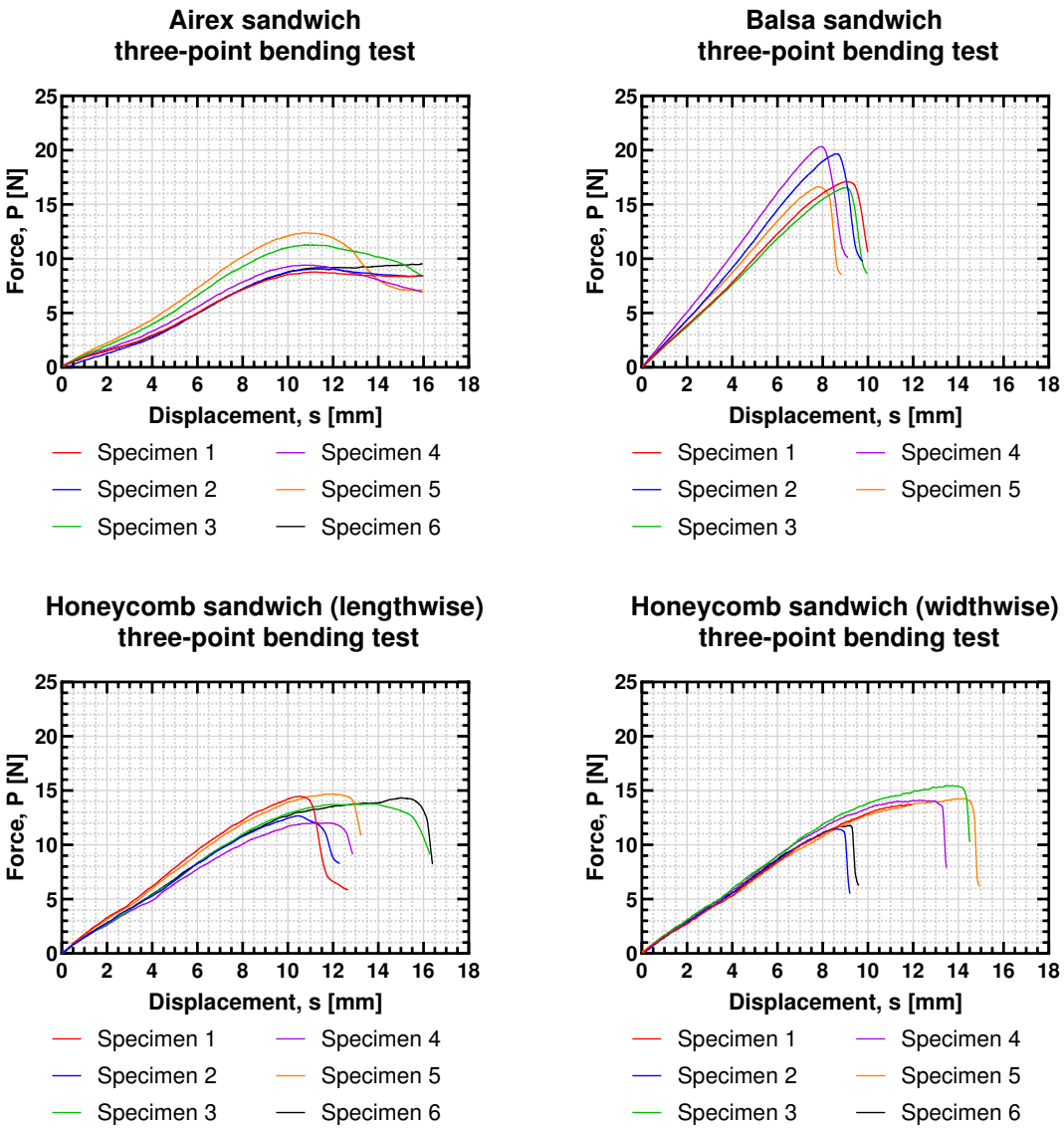

Figure 5.2: Force versus displacement curves of the four samples tested.

The AIREX® sandwich specimens showed a similar behavior when subjected to a load, and little variation in the displacement was recorded at the maximum load. As seen by the plots, the failure behavior was not catastrophic, but rather plastic, thus, allowing the structure to not fail entirely after the maximum load was recorded. The maximum recorded values were $12.61\ N$ for the load and $11.27\ mm$ for the displacement.

The balsa sandwich specimens had the highest average maximum load recorded and showed a little variation both in maximum load and displacement recorded at the maximum load. The failure behavior was slightly abrupt, as it is seen by the sudden decrease in force after the maximum load was recorded. The maximum recorded values were $20.53\ N$ for the load and $9.11\ mm$ for the displacement.

The Nomex® honeycomb lengthwise sandwich specimens showed some variation in both maximum load and displacement recorded at the maximum load, which can be explained by the irregular geometry of the honeycomb core. The results may differ if the load is applied in a zone where there are mainly hollow spaces or a zone where there is a honeycomb face. The maximum recorded values were $14.89\ N$ for the load and $15.18\ mm$ for the displacement.

The Nomex® honeycomb widthwise sandwich specimens also showed some variation in both maximum load and displacement recorded at the maximum load, which can be explained by the irregular geometry of the honeycomb core. Compared to the honeycomb oriented in the lengthwise direction, this one shows a very destructive failure due to the alignment of the core, which, in this case, makes the core shear completely. The maximum recorded values were $15.69\ N$ for the load and $13.91\ mm$ for the displacement.

Table 5.2: Average values $\bar{x}$, of the properties and dimensions obtained for each specimen of the studied sandwich samples.

Average $\bar{x}$			**Balsa**	**Airex**	**Honeycomb (L)**	**Honeycomb (W)**
Load	P_{max}	$[N]$	18.23	10.23	13.85	13.64
Mass	m_s	$[g]$	1.58	1.73	1.44	1.50
Sandwich thickness	d	$[mm]$	1.89	2.2	2.27	2.27
Core thickness	c	$[mm]$	1.71	2.03	2.08	2.05
Facing thickness	t	$[mm]$	0.0904	0.0904	0.0904	0.0904
Sandwich width	b	$[mm]$	25.05	24.94	24.88	24.86
Core shear	τ	$[MPa]$	0.2	0.10	0.13	0.13
Face bending stress	σ	$[MPa]$	11.75	53.34	70.74	71.02
Face strain	ε	$[\%]$	0.96	1.45	1.65	1.55
Deflection	s	$[mm]$	8.50	10.91	12.18	11.61
Flexural modulus	E_B	$[GPa]$	3.18	0.86	1.00	1.08
Specific strength	P_{max}/m	$[N/g]$	11.49	5.91	9.62	9.11
Specific rigidity	E_B/m	$[GPa/g]$	2.00	0.50	0.69	0.72

In Table 5.2 it is possible to get a better look at the values obtained by this experiment. The data shows the average value of a specific property or dimension measured in all the specimens tested for the different sample sandwiches.

The balsa sandwich had a higher recorded maximum load average than the rest of the samples making it also the most weight-efficient sample with a specific strength $P_{max}/m = 11.49\ N/g$ almost two times higher than the AIREX® sandwich with a specific strength $P_{max}/m = 5.91\ N/g$. Comparing the two honeycomb core sandwiches, the one oriented in the lengthwise direction shows a slightly higher specific strength.

The specific rigidity E_B/m, of the balsa sandwich, is significantly higher than the rest

of the samples with a calculated value of $2.00\ GPa$ and almost three times higher than the other samples.

The results obtained for the properties of each individual specimen can be seen in more detail from Appendix A.5 to Appendix A.8.

Table 5.3: Coefficient of variation CV, of properties and dimensions obtained for each specimen of the studied sandwich samples expressed in percentage.

Coefficient of variation CV			**Balsa**	**Airex**	**Honeycomb (L)**	**Honeycomb (W)**
Load	P_{max}	[%]	9.96	14.36	7.62	11.58
Mass	m_s	[%]	3.36	1.61	5.19	2.73
Sandwich thickness	d	[%]	2.25	0.84	0.56	0.40
Core thickness	c	[%]	2.49	0.92	0.60	0.43
Facing thickness	t	[%]	0.00	0.00	0.00	0.00
Sandwich width	b	[%]	0.44	0.52	1.23	1.19
Core shear	τ	[%]	9.37	13.28	6.57	11.65
Face bending stress	σ	[%]	9.37	13.28	6.57	11.65
Face strain	ε	[%]	5.33	2.48	14.81	19.17
Deflection	s	[%]	7.19	2.56	15.05	18.08
Flexural modulus	E_B	[%]	10.83	13.34	13.30	9.22
Specific strength	P_{max}/m	[%]	6.62	14.62	4.25	11.08
Specific rigidity	E_B/m	[%]	7.87	13.85	12.25	9.47

Table 5.2 represents the coefficient of variation CV, for the values obtained by this experiment, where higher values represent large dispersion in the obtained data and smaller values represent similar data obtained for a specific property or dimension.

The AIREX® sandwich measurements for the maximum load recorded P_{max} showed a significant high dispersion but the opposite is observed for the deflection recorded at the maximum load s, where the coefficient of variation is very low.

The balsa sandwich specimens showed low values of dispersion with every property or dimension getting a value of CV below 10%, besides the flexural modulus which barely passed this value.

Both the Nomex® honeycomb sandwiches show some variation in the data obtained, not so much in the maximum load recorded, but in the deflection recorded at the maximum load where the widthwise honeycomb reached a value of 18.08%.

Table 5.4: Properties and dimensions obtained in the three-point bending test of the carbon fiber laminate specimens.

Carbon fiber laminates			**Specimen 1**	**Specimen 2**
Load	P_{max}	$[N]$	43.27	41.81
Thickness	h	$[mm]$	1.98	1.99
Width	b	$[mm]$	15.12	15.16
Flexural stress	σ_f	$[MPa]$	87.59	83.58
Deflection	s	$[mm]$	19.50	19.17
Flexural modulus	E_B	$[GPa]$	4.96	4.39

Table 5.4 shows the results obtained for the three-point bending test of the carbon fiber laminate specimens according to the guidelines shown in Section 3.2.2.2. The data collected is represented in Figure 5.3 by the force vs displacement for each specimen.

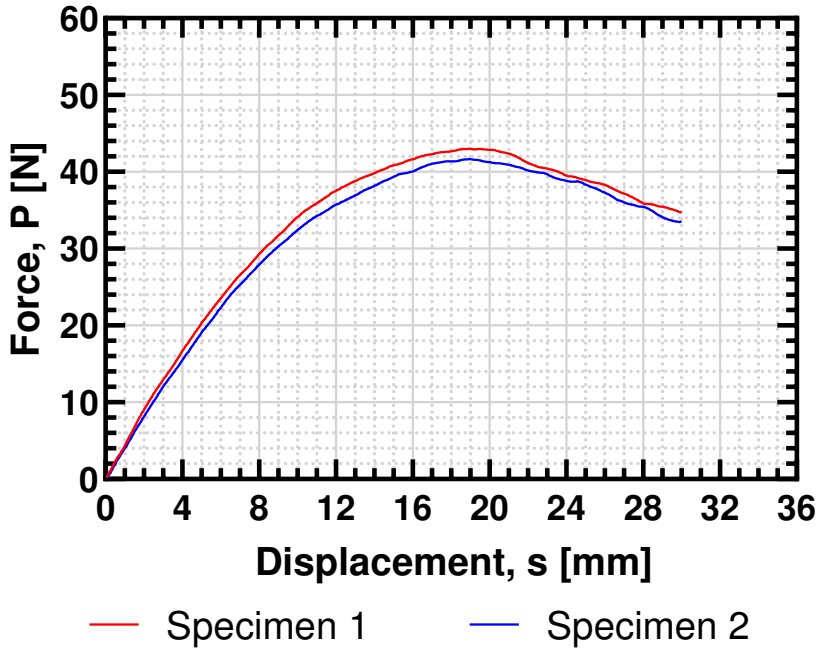

Figure 5.3: Force versus displacement curves of the carbon fiber laminates specimens three-Point bending test with the two specimens labeled from 1 to 2.

Both the specimens did not suffer a specific failure mode but instead kept on bending. A more abrupt failure was expected since carbon fiber normally acts in a less elastic behavior. These two sets of specimens were produced during the winter season when the laboratory reaches low temperatures, and although efforts were made to elevate the temperature by improvising a warm housing, the curing of the specimens might have been affected and thus the mechanical properties of the laminates decreased.

The data collected from the FEA is represented in Figure 5.4 by the force versus displacement plots for each sample in their elastic region.

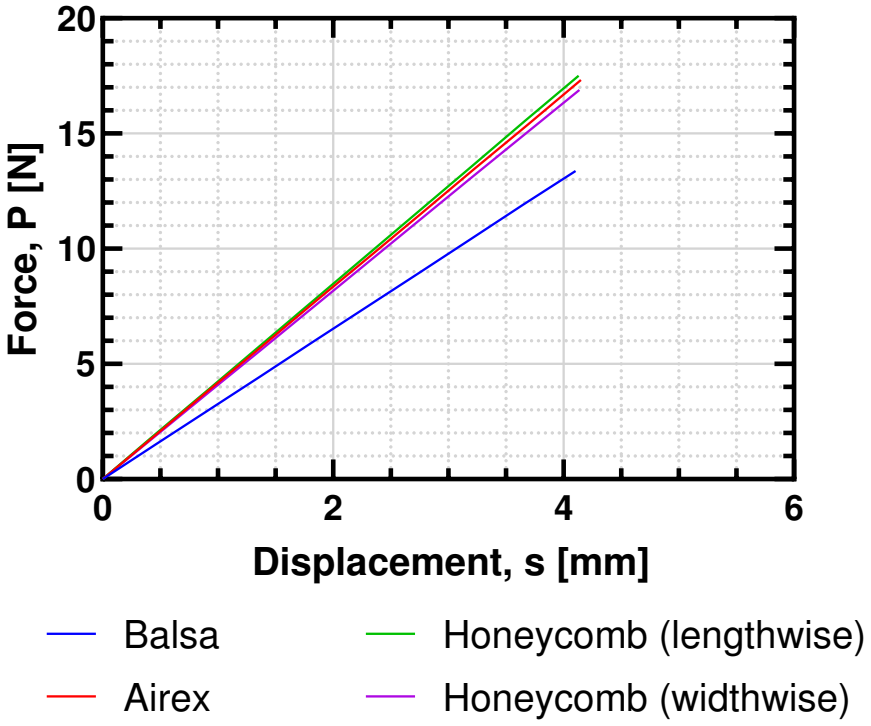

Figure 5.4: Force versus displacement curves of the samples tested in the software ANSYS®.

The results show that the FEA was not able to predict the behavior of the samples during the three-point bending test made in the laboratory. These results can be explained by the inaccurate properties values of the materials used in the simulation which did not represent the real properties of the carbon fiber cloth used to run the experimental procedure. These results seem to reflect a correlation between the sandwich thickness and its strength as both the AIREX® and Honeycomb have similar thicknesses and the balsa sandwich is the one with the lowest thickness, which means that most probably, the core had little impact on the results and the carbon facings were defined with properties above the real value. The results obtained on the FEA also show a less flexible behavior for the sandwich composites, which can be seen by the smaller deflection obtained when compared to the experimental results. This might be due to the bad curing of the sandwich composites which resulted in a more flexible structure.

The carbon fiber laminate results of the FEA also gave a higher result than expected, which confirms that the properties used for the carbon fiber cloth were lower than the ones used to perform the FEA.

Chapter 6

Conclusion

This chapter has the main purpose of giving an overview of the conclusions taken from the work done and giving guidelines for future work.

Section 6.1 - **Overview**, summarizes all the work done in this paper, followed procedures, results and also the drawbacks encountered.

Section 6.2 - **Future work**, suggests a path for future work in this topic and complementary subjects capable of generating new lines of work research.

6.1 Overview

The search for better materials and structures to optimize flight performance will always be present side-by-side with the evolution of aerospace and aeronautical fields.

Throughout this work, different sandwich composite structures were compared to select the lighter solution in order to reduce the overall weight of the wing skin without compromising its strength. For that, many combinations of a low surface mass carbon fiber facing and a core material were studied. The core materials used are well-known in the aeronautical industry and have always been subjected to large demand due to their good overall properties. These core materials are the following:

- Balsa wood
- AIREX®
- Nomex® honeycomb

In order to test the sandwich composite structures, three-point bending tests were carried out according to standard procedures and subsequently, data such as force, deflection, and failure modes were recorded.

Three-point bending tests were also carried out to evaluate the flexural properties of carbon fiber laminates. The data collected can be seen in Table 5.4.

To compare the four samples (balsa wood, airex, and honeycomb in the lengthwise and widthwise directions) two important parameters, which can be seen in Table 5.2, were calculated. The first one is the specific strength [N/g] is a measure of how much force the sample can hold per gram of weight, and the highest the value, the lighter a structure can be without compromising its weight. The second one is the specific rigidity [GPa/g] which measures

the ability of the material to resist deformation when bending per gram of weight and the highest the value, the less bending will occur without compromising its weight.

FEA were also performed in order to validate the results obtained experimentally. Unfortunately, these results diverged from the ones obtained in the laboratory, and in general, higher flexural resistance was observed in the FEA. Some of the reasons for this divergence in results might be explained by the following hypothesis:

- Lack of data on the elastic or mechanical properties of the dry carbon fiber fabric used;
- Bad curing of the specimens and, as a result, inferior properties of the sandwich samples;

Even though the FEA results were not satisfactory, the experimental procedures and experiments were successfully performed and enough data was collected in order to take conclusions concerning the use of the most adequate lightweight sandwich structure for UAV wings.

It is possible to conclude that, in general, the balsa wood sandwich is the best composite sandwich structure. When compared to the others, it showed higher specific strength and higher specific rigidity. Even though its price is higher than the AIREX® sandwich it comes very close to the Nomex® honeycomb sandwich, which still makes a good option when considering a compromise between cost and strength.

6.2 Future work

After an in-depth analysis of the state of the art, thoughtful consideration about the work done in this thesis, the results it gave, and also the drawbacks encountered, suggestions for future work have aroused. As follows, these suggestions are given as means to complement the research done in this work and generate new lines of research:

- Conducting an extensive evaluation of the elastic, plastic, and mechanical properties of the carbon fiber laminate used in this experiment;
- Producing similar samples to the ones shown in this work in an environment with more pressure and temperature control;
- A study about the effect of different curing temperatures on the properties of the composite sandwich samples;
- Producing and testing new combinations of facing and core materials and also experiment different weave patterns;

Bibliography

[1] Mar-Bal, Inc. (2018) History of composites. [Online]. Available: https://www.mar-bal.com/language/en/applications/history-of-composites/ 1

[2] W. D. Callister, D. G. Rethwisch *et al.*, *Materials science and engineering: an introduction*. Wiley New York, 2018, vol. 9. 2

[3] M. Rzeszutek, M. Lis-Turlejska, A. Krajewska, A. Zawadzka, M. Lewandowski, and S. Szumiał, "Long-term psychological consequences of world war ii trauma among polish survivors: A mixed-methods study on the role of social acknowledgment," *Frontiers in Psychology*, vol. 11, p. 210, 2020.

[4] Wikipedia, the free encyclopedia. (2022) De havilland mosquito. [Online]. Available: https://en.wikipedia.org/wiki/De_Havilland_Mosquito 2

[5] O. Nakamura, T. Ohana, M. Tazawa, S. Yokota, W. Shinoda, and J. ITOH, "Study on the pan carbon-fiber-innovation for modeling a successful r&d management—an excited-oscillation management model—," *Synthesiology English edition*, vol. 2, no. 2, pp. 154–164, 2009. 3

[6] J. M. Davies, *Lightweight sandwich construction*. John Wiley & Sons, 2008. 3

[7] A. P. Mouritz, *Introduction to aerospace materials*. Elsevier, 2012. 3, 19

[8] W. G. Roeseler, B. Sarh, M. U. Kismarton, J. Quinlivan, J. Sutter, and D. Roberts, "Composite structures: the first 100 years," in *16th International Conference on Composite Materials*. Japan Society for Composite Materials Kyoto, Japan, 2007, pp. 1–41. 4

[9] Baykar Technology. (2022) Bayraktar tb2. [Online]. Available: https://www.baykartech.com 4

[10] Polaris Market Research. (2021) Advanced composites market size: Global industry report, 2021 - 2028. [Online]. Available: https://www.polarismarketresearch.com/industry-analysis/advanced-composites-market 5

[11] A. Al-Fatlawi, K. Jármai, and G. Kovács, "Optimal design of a fiber-reinforced plastic composite sandwich structure for the base plate of aircraft pallets in order to reduce weight," *Polymers*, vol. 13, no. 5, p. 834, 2021. 8

[12] A. Granta. (2017) Material property charts. [Online]. Available: https://www.grantadesign.com/education/students/charts/ 9, 10

[13] L. Xu, Y. Huang, C. Zhao, and S. K. Ha, "Progressive failure prediction of woven fabric composites using a multi-scale approach," *International Journal of Damage Mechanics*, vol. 27, no. 1, pp. 97–119, 2018. 11

[14] Van Paepegem. (2021) Home made composites (hommacom) - what are composites ? [Online]. Available: https://composites.ugent.be/home_made_composites/what_are_composites.html 11

[15] Z. Hasan, *Tooling for Composite Aerospace Structures: Manufacturing and Applications*, ser. ISBN: 978-0-12-819957-2. Butterworth-Heinemann, 2020. 12

[16] E. Asmatulu, A. Alonayni, and M. Alamir, "Safety concerns in composite manufacturing and machining," in *Behavior and Mechanics of Multifunctional Materials and Composites XII*, vol. 10596. SPIE, 2018, pp. 421–428. 12

[17] O. T. Thomsen, E. Bozhevolnaya, and A. Lyckegaard, *Sandwich Structures 7: Advancing with Sandwich Structures and Materials: Proceedings of the 7th International Conference on Sandwich Structures, Aalborg University, Aalborg, Denmark, 29-31 August 2005*. Springer Science & Business Media, 2005. 13

[18] D. B. Miracle, S. L. Donaldson, S. D. Henry, C. Moosbrugger, G. J. Anton, B. R. Sanders, N. Hrivnak, C. Terman, J. Kinson, K. Muldoon *et al.*, *ASM handbook*. ASM international Materials Park, OH, 2001, vol. 21. 13, 14

[19] P. K. Mallick, *Fiber-reinforced composites: materials, manufacturing, and design*. CRC press, 2007. 15, 16

[20] U. States, *Advanced Materials by Design*. NTIS, 1998. 15

[21] I. M. Daniel, O. Ishai, I. M. Daniel, and I. Daniel, *Engineering mechanics of composite materials*. Oxford university press New York, 2006, vol. 1994. 15, 16

[22] S. Gurit, "Guide to composites," *Published by SP Gurit*, 2016. 17, 18, 19, 20

[23] G. Pohl and M. Pfalz, "Innovative composite-fibre components in architecture," in *Textiles, Polymers and Composites for Buildings*. Elsevier, 2010, pp. 420–470. 18

[24] S. Joshi, "The pultrusion process for polymer matrix composites," in *Manufacturing techniques for polymer matrix composites (PMCs)*. Elsevier, 2012, pp. 381–413. 19

[25] E. Gdoutos and I. Daniel, "Failure mechanisms of composite sandwich structures," *Proceedings of the Academy of Athens*, vol. 84, pp. 478–469, 2009. 20

[26] I. M. Daniel, E. E. Gdoutos, J. L. Abot, and K.-A. Wang, "Deformation and failure

of composite sandwich structures," *Journal of Thermoplastic Composite Materials*, vol. 16, no. 4, pp. 345–364, 2003. 21

[27] R. P. Ley, W. Lin, and U. Mbanefo, "Facesheet wrinkling in sandwich structures," Nasa, Tech. Rep., 1999. 21

[28] E. Linul and L. Marsavina, "Mechanical characterization of rigid pur foams used for wind turbine blades construction," *Recent Advances in Composite Materials for Wind Turbines Blades; WAP-AMSA*, 2013. 21, 22, 23

[29] A. Petras and M. Sutcliffe, "Failure mode maps for honeycomb sandwich panels," *Composite structures*, vol. 44, no. 4, pp. 237–252, 1999. 21, 22

[30] M. F. Ashby and L. J. Gibson, *Cellular solids: structure and properties*. John Wiley & Sons, 1997. 21, 22

[31] F. Shuaeib and P. Soden, "Indentation failure of composite sandwich beams," *Composites science and Technology*, vol. 57, no. 9-10, pp. 1249–1259, 1997. 22

[32] I. Odessa, Y. Frostig, and O. Rabinovitch, "Dynamic interfacial debonding in sandwich panels," *Composites Part B: Engineering*, vol. 185, p. 107733, 2020. 23

[33] P. Santos, P. Gamboa, P. Santos, and J. Silva, "Structural design of a composite variable-span wing," pp. 23–27, 2013. 27

[34] M. K. Egbo, "A fundamental review on composite materials and some of their applications in biomedical engineering," *Journal of King Saud University-Engineering Sciences*, vol. 33, no. 8, pp. 557–568, 2021. 29

[35] C. Astm, "393, standard test. method for flexural properties of sandwich constructions," *American Society for Testing and Materials Annual Book of ASTM Standards: West Conshohocken, PA, USA*, 2000. 30, 32

[36] B. Standard and B. ISO, "Fibre-reinforced plastic composites—determination of flexural properties," *BS EN ISO*, vol. 14125, 1998. 33, 34

[37] A. Da Silva and S. Kyriakides, "Compressive response and failure of balsa wood," *International Journal of Solids and Structures*, vol. 44, no. 25-26, pp. 8685–8717, 2007. 37

[38] R. Composite. (2013) Composite manufacturer. [Online]. Available: https://www.r-g.de/en/home.html 39

[39] Siemens. (2022) Finite element analysis. [Online]. Available: https://www.plm.

automation.siemens.com/global/en/our-story/glossary/finite-element-analysis-fea/13173 43

Appendix A

Appendix

A.1 Balsa wood sandwich specimens three-point bending test

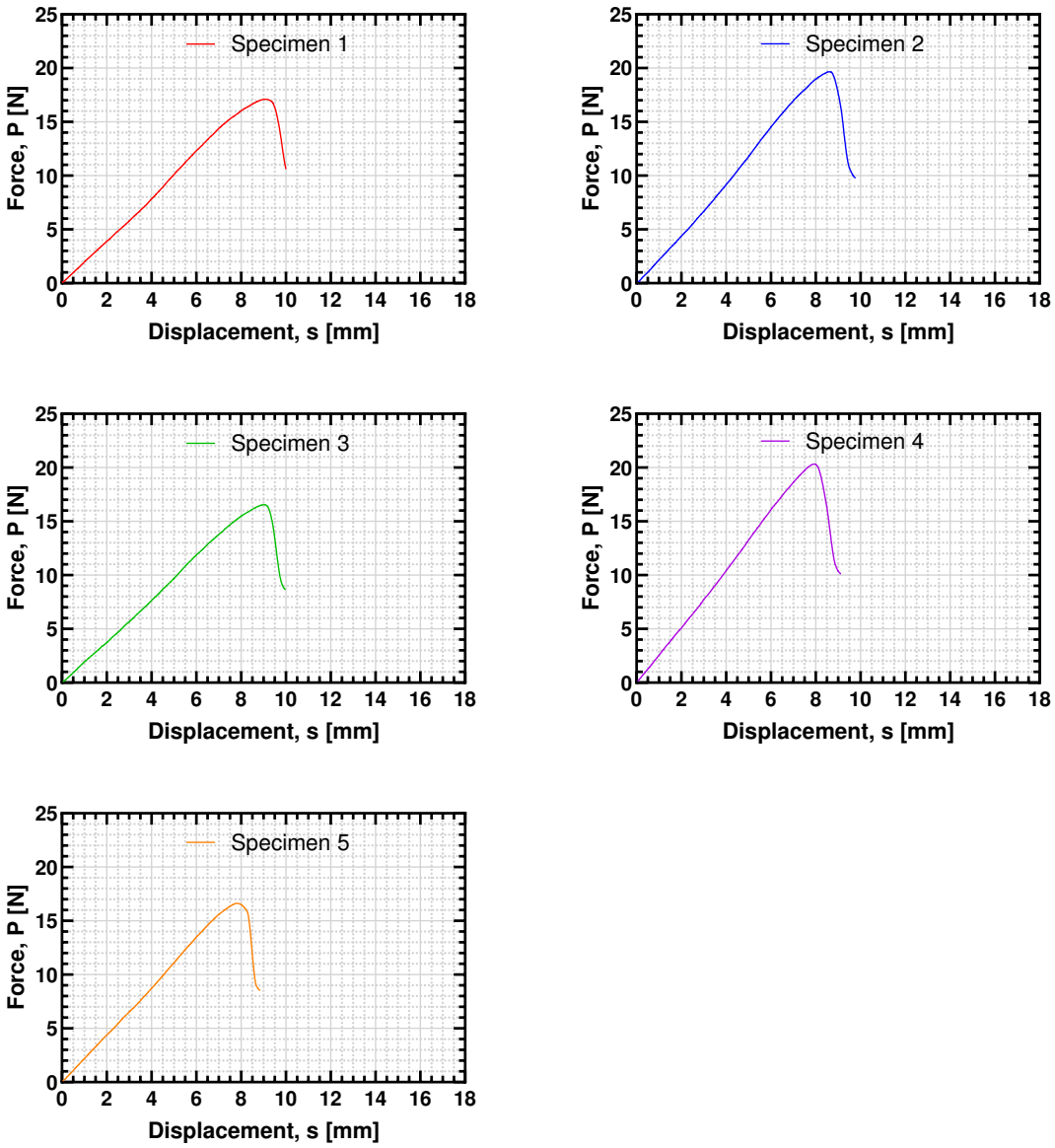

Figure A.1: Force versus displacement curves of the balsa wood sandwich specimens three-Point bending test with the six specimens labeled from 1 to 5.

A.2 AIREX® C 70.75 sandwich specimens three-point bending test

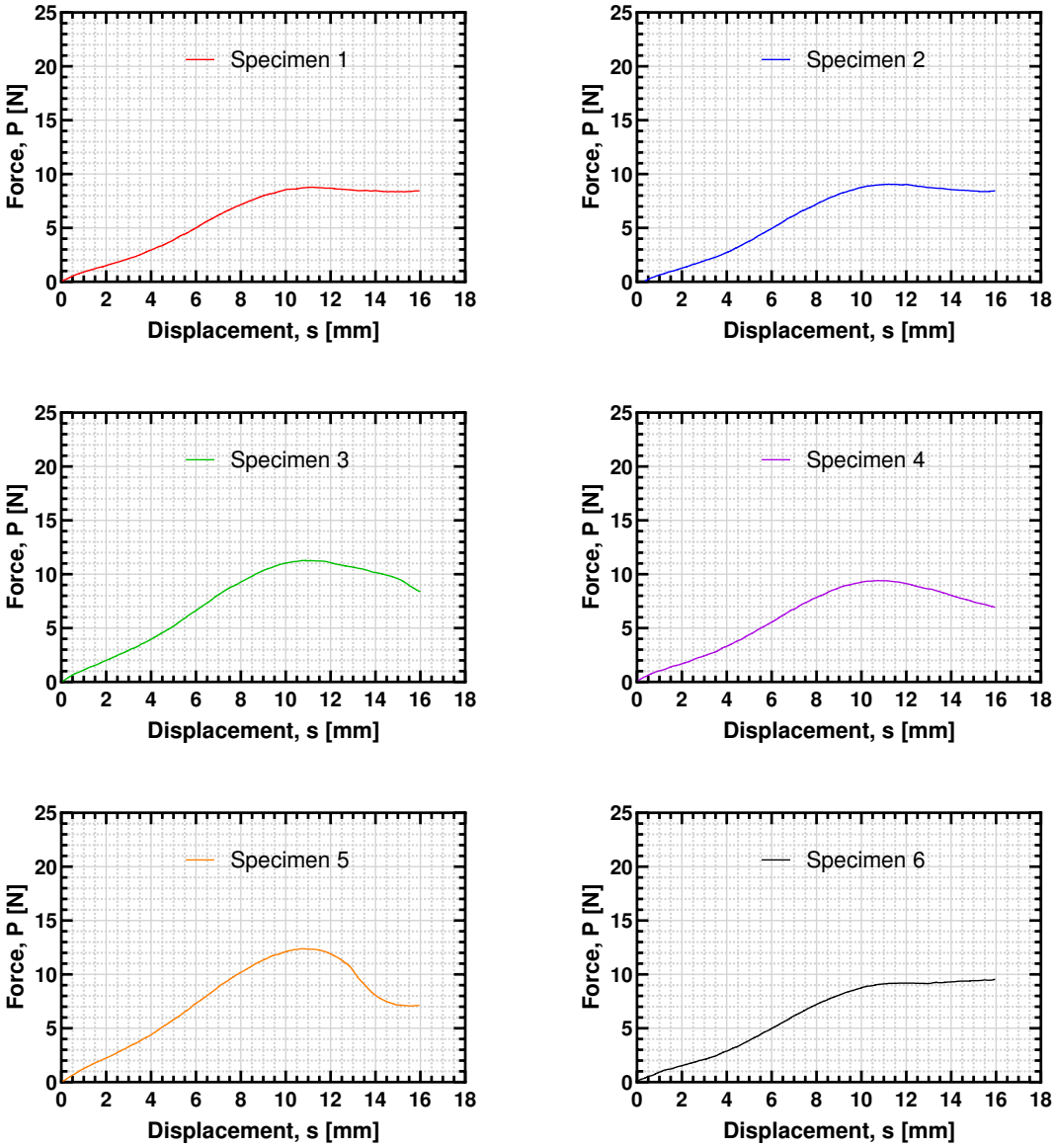

Figure A.2: Force versus displacement curves of the AIREX® C 70.75 sandwich specimens three-Point bending test with the six specimens labeled from 1 to 6.

A.3 Honeycomb sandwich (lengthwise) specimens three-point bending test

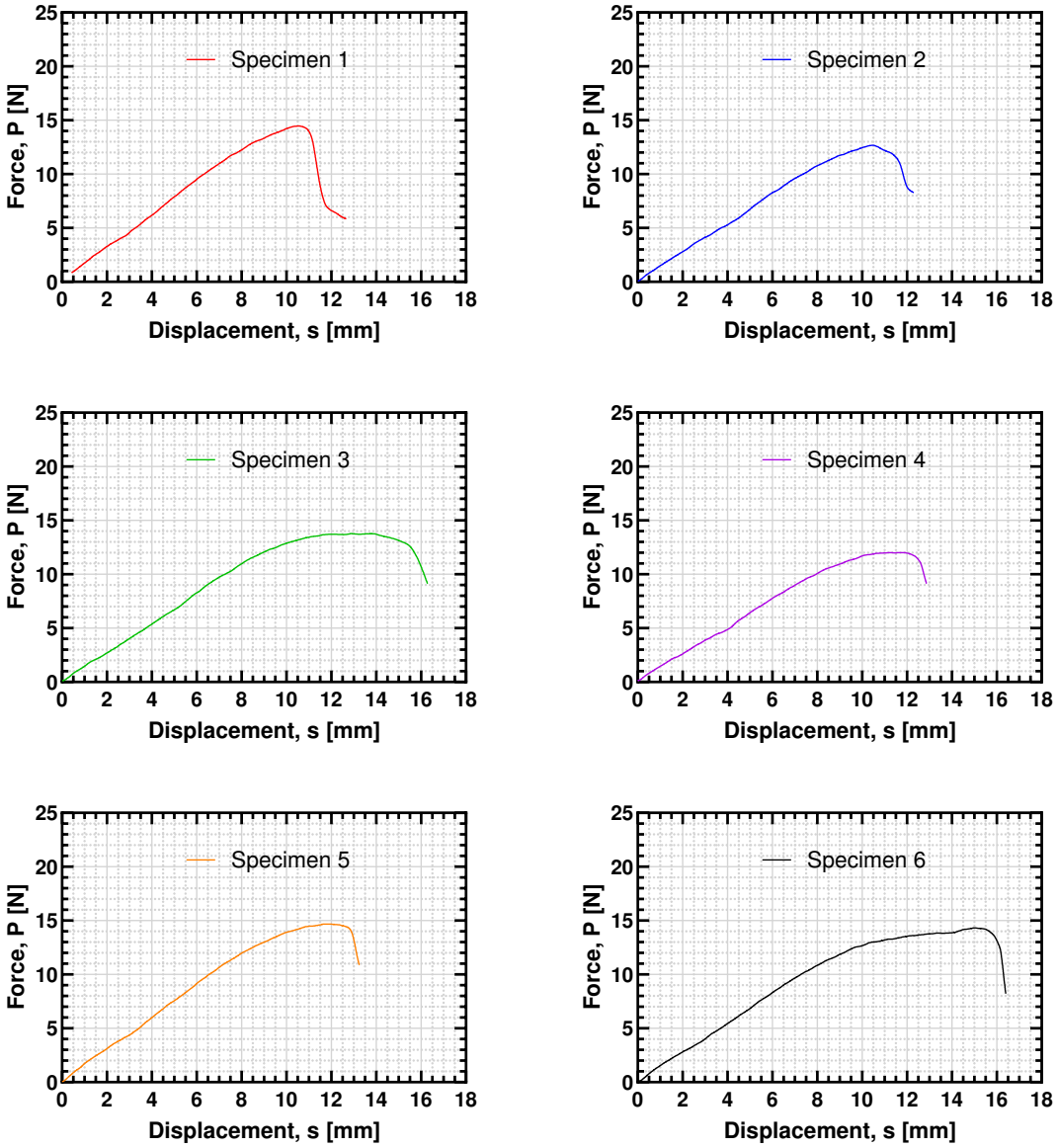

Figure A.3: Force versus displacement curves of the honeycomb sandwich (lengthwise) specimens three-Point bending test with the six specimens labeled from 1 to 6.

A.4 Honeycomb sandwich (widthwise) specimens three-point bending test

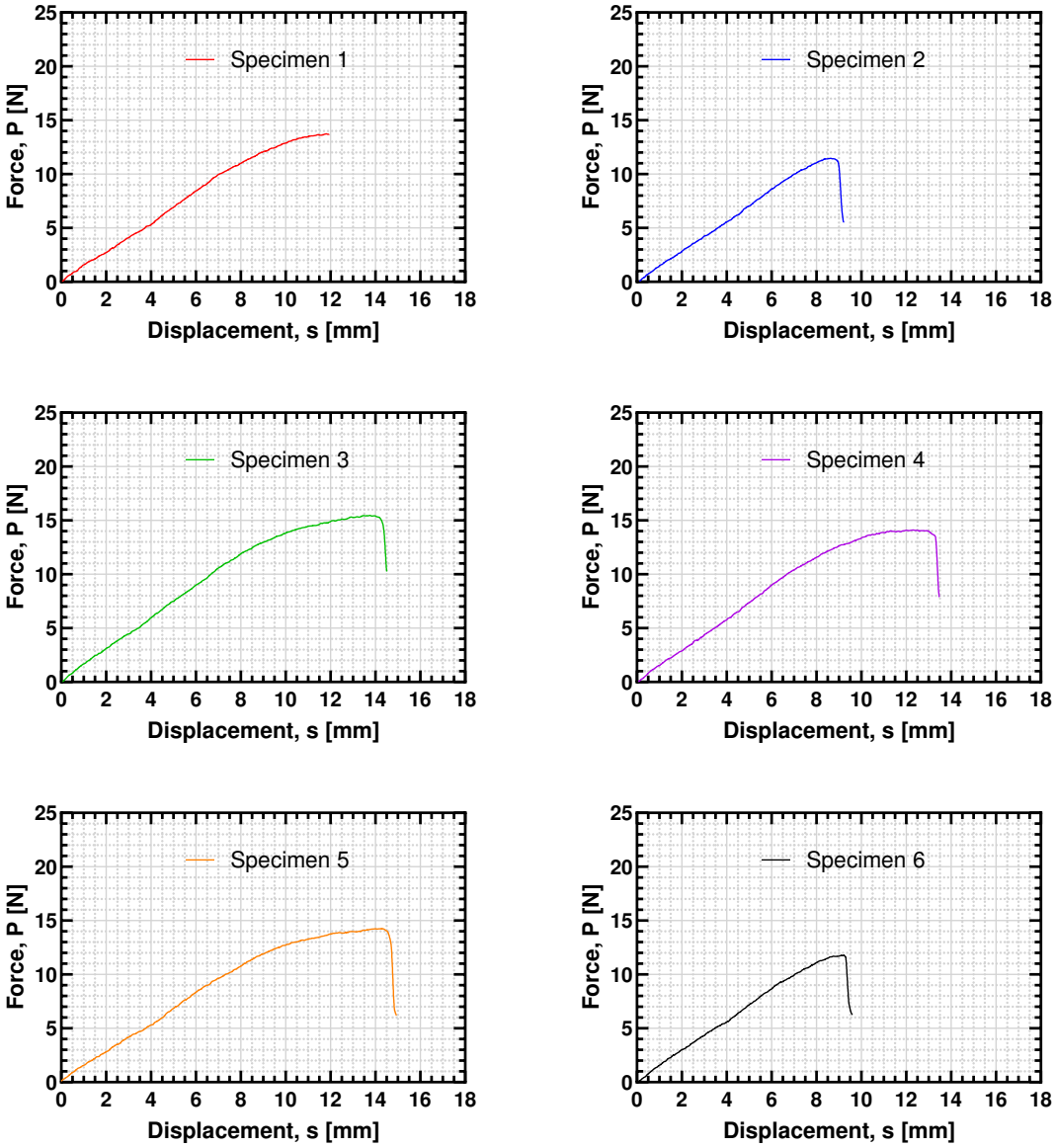

Figure A.4: Force versus displacement curves of the honeycomb sandwich (widthwise) specimens three-Point bending test with the six specimens labeled from 1 to 6.

A.5 Balsa wood sandwich specimen properties and dimensions

Table A.5: Properties and dimensions obtained for each balsa wood sandwich specimen.

Balsa specimens								
Specimen number			**1**	**2**	**3**	**4**	**5**	**6**
Load	P_{max}	$[N]$	17.30	19.84	16.72	20.53	16.77	D
Mass	m_s	$[g]$	1.55	1.62	1.55	1.66	1.54	D
Sandwich thickness	d	$[mm]$	1.83	1.88	1.89	1.94	1.93	D
Core thickness	c	$[mm]$	1.65	1.69	1.71	1.75	1.75	D
Facing thickness	t	$[mm]$	0.09	0.09	0.09	0.09	0.09	D
Sandwich width	b	$[mm]$	24.92	25.22	25.07	25.01	25.05	D
Core shear	τ	$[MPa]$	0.2	0.22	0.19	0.22	0.18	D
Face bending stress	σ	$[MPa]$	110.34	121.93	102.64	123.10	100.75	D
Face strain	ε	$[\%]$	1.00	0.97	1.02	0.92	0.91	D
Deflection	s	$[mm]$	9.11	8.65	9.03	7.89	7.83	D
Flexural modulus	E_B	$[GPa]$	3.11	3.45	2.75	3.59	2.98	D
Specific strength	P_{max}/m	$[N/g]$	11.16	12.25	10.79	12.37	10.89	D
Specific rigidity	E_B/m	$[GPa/g]$	2.00	2.13	1.77	2.16	1.94	D

D - Damaged specimen and therefore, no reliable data extracted from it.

A.6 AIREX® C 70.75 sandwich specimen properties and dimensions

Table A.6: Properties and dimensions obtained for each AIREX® C 70.75 sandwich specimen.

AIREX® C 70.75 specimens								
Specimen number			**1**	**2**	**3**	**4**	**5**	**6**
Load	P_{max}	$[N]$	8.95	9.28	11.50	9.63	12.61	9.44
Mass	m_s	$[g]$	1.74	1.76	1.73	1.68	1.73	1.75
Sandwich thickness	d	$[mm]$	2.20	2.21	2.22	2.20	2.25	2.21
Core thickness	c	$[mm]$	2.02	2.03	2.04	2.02	2.07	2.03
Facing thickness	t	$[mm]$	0.09	0.09	0.09	0.09	0.09	0.09
Sandwich width	b	$[mm]$	24.91	24.92	24.77	25.02	25.15	24.89
Core shear	τ	$[MPa]$	0.085	0.088	0.109	0.091	0.116	0.089
Face bending stress	σ	$[MPa]$	47.18	48.59	60.29	50.38	64.20	49.41
Face strain	ε	$[\%]$	1.44	1.49	1.43	1.40	1.44	1.50
Deflection	s	$[mm]$	10.93	11.21	10.76	10.58	10.70	11.27
Flexural modulus	E_B	$[GPa]$	0.77	0.77	0.99	0.85	1.03	0.78
Specific strength	P_{max}/m	$[N/g]$	5.15	5.27	6.65	5.73	7.29	5.39
Specific rigidity	E_B/m	$[GPa/g]$	0.45	0.44	0.57	0.51	0.59	0.44

A.7 Honeycomb sandwich (lengthwise) sandwich specimen properties and dimensions

Table A.7: Properties and dimensions obtained for each honeycomb sandwich (lengthwise) sandwich specimen.

Honeycomb sandwich (lengthwise) specimens								
Specimen number			**1**	**2**	**3**	**4**	**5**	**6**
Load	P_{max}	$[N]$	14.59	12.94	13.97	12.22	14.89	14.50
Mass	m_s	$[g]$	1.48	1.40	1.38	1.35	1.55	1.47
Sandwich thickness	d	$[mm]$	2.27	2.27	2.25	2.26	2.29	2.26
Core thickness	c	$[mm]$	2.09	2.08	2.07	2.08	2.10	2.08
Facing thickness	t	$[mm]$	0.09	0.09	0.09	0.09	0.09	0.09
Sandwich width	b	$[mm]$	24.91	24.97	24.76	24.36	25.03	25.28
Core shear	τ	$[MPa]$	0.13	0.12	0.13	0.12	0.14	0.13
Face bending stress	σ	$[MPa]$	74.25	65.89	72.33	63.94	74.98	73.04
Face strain	ε	$[\%]$	1.43	1.44	1.82	1.57	1.61	2.06
Deflection	s	$[mm]$	10.46	11.59	13.51	11.57	11.75	15.18
Flexural modulus	E_B	$[GPa]$	1.19	1.05	0.92	0.94	1.06	0.82
Specific strength	P_{max}/m	$[N/g]$	9.86	9.24	10.12	9.05	9.61	9.86
Specific rigidity	E_B/m	$[GPa/g]$	0.81	0.75	0.67	0.70	0.68	0.55

A.8 Honeycomb sandwich (widthwise) sandwich specimen properties and dimensions

Table A.8: Properties and dimensions obtained for each honeycomb sandwich (widthwise) sandwich specimen.

Honeycomb sandwich (widthwise) specimens								
Specimen number			**1**	**2**	**3**	**4**	**5**	**6**
Load	P_{max}	$[N]$	13.94	11.58	15.69	14.30	14.42	11.94
Mass	m_s	$[g]$	1.53	1.45	1.53	1.51	1.44	1.52
Sandwich thickness	d	$[mm]$	2.22	2.22	2.23	2.23	2.24	2.22
Core thickness	c	$[mm]$	2.04	2.04	2.05	2.05	2.06	2.04
Facing thickness	t	$[mm]$	0.09	0.09	0.09	0.09	0.09	0.09
Sandwich width	b	$[mm]$	24.58	24.81	24.85	25.24	24.53	25.18
Core shear	τ	$[MPa]$	0.13	0.11	0.15	0.13	0.14	0.11
Face bending stress	σ	$[MPa]$	73.72	60.61	81.50	73.13	75.64	61.49
Face strain	ε	$[\%]$	1.57	1.17	1.84	1.63	1.87	2.23
Deflection	s	$[mm]$	11.80	8.80	13.75	12.18	13.91	9.19
Flexural modulus	E_B	$[GPa]$	1.10	1.21	1.03	1.04	0.94	1.17
Specific strength	P_{max}/m	$[N/g]$	9.11	7.98	10.25	9.47	10.02	7.85
Specific rigidity	E_B/m	$[GPa/g]$	0.72	0.84	0.67	069	0.65	0.77